10-16-2018

A Regional Survey of River-plume Sedimentation on the Mississippi River Delta Front

Andrew J. Courtois
Louisiana State University and Agricultural and Mechanical College

A REGIONAL SURVEY OF RIVER-PLUME SEDIMENTATION ON THE MISSISSIPPI RIVER DELTA FRONT

A Thesis

Submitted to the Graduate Faculty of the
Louisiana State University and
Agricultural and Mechanical College
in partial fulfillment of the
requirements for the degree of
Master of Science

in

The Department of Geology and Geophysics

by
Andrew Courtois
B.S., University of New Orleans, 2016
December 2018

Acknowledgements

I would like to thank the Bureau of Ocean Energy Management for funding this project and the United States Geological Survey for providing multiple data sets. I would also like to thank the Louisiana State University Dept. of Geology and Geophysics for additional funding.

I would like to give Samuel Bentley a special thanks for providing excellent advisement throughout my research as well as giving me the opportunity to work on this project. A special thanks to Michael Miner for the introduction to Sam and the valuable input you have given me. Thank you to Ioannis Georgiou and Kehui Xu for serving on my committee and providing helpful feedback through this process. I would like to give a special thanks to Kanchan Maiti for the valuable feedback you gave over the course of several discussions. Thank you to everyone from the Bentley lab group, you have all been a tremendous help and special thanks to Giancarlo Restreppo for your much appreciated input on several occasions.

Lastly, I would like to thank my wife and family. You all have been very supportive throughout this entire process and I am sincerely grateful.

Table of Contents

Illustrations

List of Tables

List of Figures

List of Abbreviations

Disintegrations per minute per square centimeter (dpm/cm^2)

Disintegrations per minute per cubic centimeter (dpm/cm^3)

Disintegrations per minute per gram (dpm/g)

Gully (gul)

Lobe (lob)

Mississippi River (MR)

Mississippi River Delta (MRD)

Mississippi River Delta Front (MRDF)

Pass a Loutre (PAL)

Prodelta (pro)

Sediment Deposition Rate (SDR)

South Pass (S Pass)

Southwest Pass (SW Pass)

Undisturbed seafloor (und)

Abstract

Many studies of the Mississippi River Delta (MRD) have shown historic declines in sediment load over the last few decades. Recent studies also reported that ~50% of the suspended load during floods is sequestered within the delta. While the impact of declining sediment load on wetland loss is relatively well documented, submarine sedimentary processes on the delta front during this recent period of are understudied. To better understand modern sediment dispersal and deposition across the Mississippi River Delta Front, 31 multicores were collected in June 2017 from locations extending offshore from the main river outlets in water depths of 25-280 m. Core locations were selected based on multibeam bathymetric and morphological data collected by the USGS in May 2017; the timing of collection coincided with the end of annual peak discharge on the Mississippi River. This collaborative multi-agency survey is the first to study delta-front sedimentary processes regionally with a wide suite of geophysical and coring tools. Core locations included the dominant depositional environments: mudflow lobes, gullies, and undisturbed prodelta. Nine multicores were subsampled at 2 cm intervals and analyzed for Beryllium-7 activity and 4 cores were subsampled for excess Thorium-234 activity via gamma spectrometry. Grain-size analysis and X-radiography were performed on cores as well. Results indicate a general trend of declining Be-7 activity with increasing distance from source, and in deeper water. Inshore samples near Southwest Pass show the highest Be-7 inventories and deepest penetration depth of Be-7 into the sediment (24-26 cm), which is a preliminary indicator of rapid seasonal sedimentation. Sediment focusing was determined at mudflow gully and lobe locations throughout the delta front. X-radiography revealed that the likelihood of preserving bedding layers occurs proximal to river-mouth while a trend is observed of increased bioturbation offshore. Sediment dispersal remains detectable offshore from all three major river

outlets, despite overall decline of sediment load in recent decades, and pronounced declines for South Pass and Pass a Loutre. Future research should focus on relationships among changing sediment loads, dispersal patterns, and sediment transport by mudflows, which are an important process for dispersal after initial deposition.

Chapter 1. Introduction

The Mississippi River Delta Front (MRDF) is an area extending offshore of the Mississippi River Delta (MRD) in water depths of 10-250 m with distinct morphological features related to gravity-driven sediment transport (Figure 1). It is an area of valuable economic importance in terms of marine transportation, fisheries, and the oil and gas industry. Sediment supply, waves, and tides have strong influences on morphology and stratigraphy in areas proximal to deltaic systems (Walsh and Nittrouer, 2009). In addition, much research has studied the significant effect that submarine mass wasting has on the MRDF (Coleman et al., 1974; Prior and Suhayda, 1979; Coleman et al., 1980; Obelcz et al., 2017; Maloney et al., 2018).

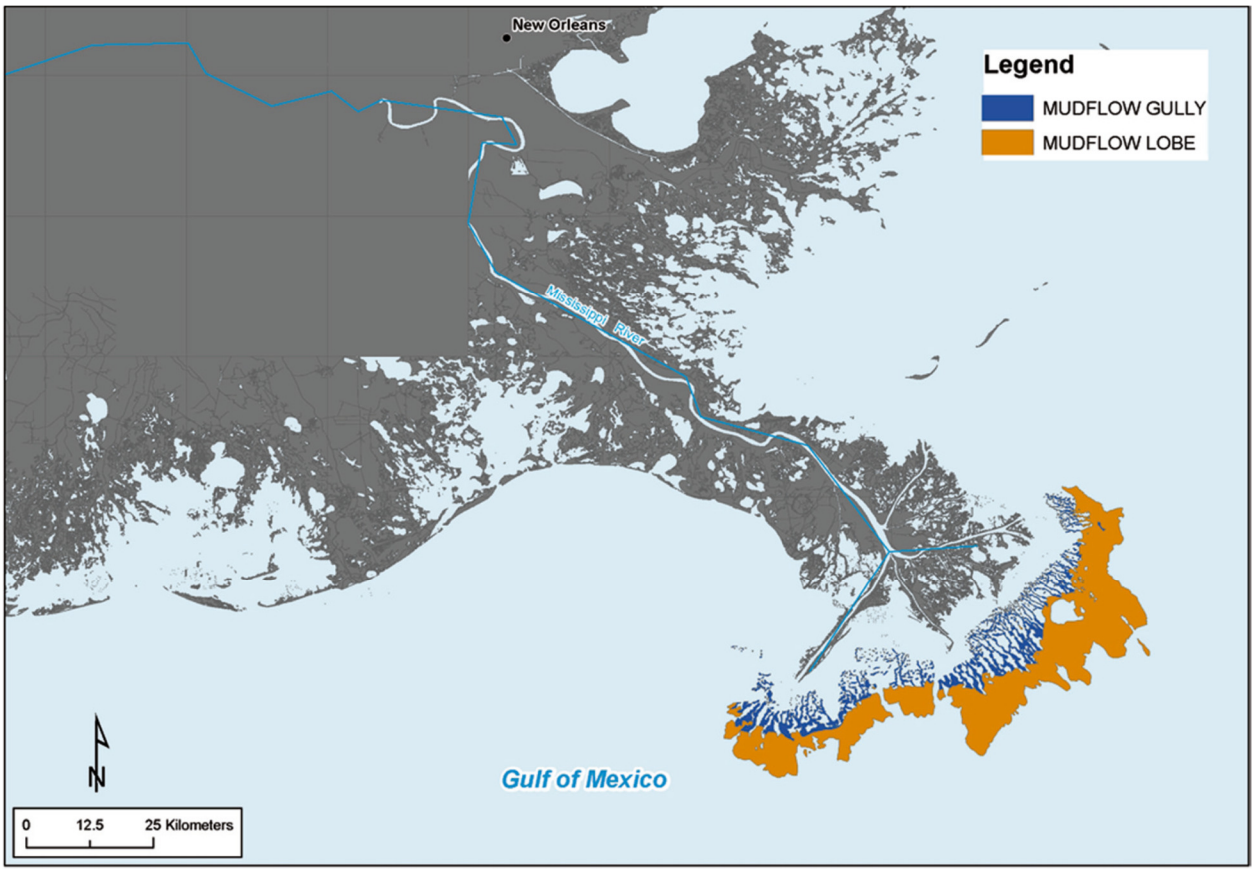

Figure 1. Regional map of MRDF. Map of mudflow gullies (blue) and lobes (orange) surrounding the Mississippi River Delta Front (Hitchcock et al., 2010).

Submarine landslides are prone throughout the area posing a significant hazard to oil and gas infrastructure. The modern MRD region contains infrastructure responsible for nearly 25% of US hydrocarbon production (Blum and Roberts, 2012). The impact of these failures have been known since the 1970s (Bea, 1971). The mass movement of sediment along the MRDF can be triggered by a variety of different mechanisms, with the passage of hurricanes as a primary cause (Coleman, 1988). Hurricane Ivan, in 2004, triggered a slope failure in waters offshore of South Pass damaging a Taylor Energy platform. For the sake of offshore structures, such as oil and gas infrastructure, it is imperative that these features and the processes that govern them be understood (Prior and Suhayda, 1979).

Besides the passage of hurricanes, rapid sedimentation along the MRDF is a contributing factor to submarine landslides (Coleman, 1988). Regions of active sedimentation along the delta front experience high sedimentation rates, even with the pronounced historical decline in sediment load of the Mississippi River (MR). Changes in sediment load of the MR and redistribution of the load among the dominant river passes affect the deposition of sediment along the MRDF, making past studies measuring sedimentation rates along the continental shelf proximal to the delta outdated over short periods of time. To better assess the risk of submarine landslides on the MRDF, a regional survey was done to observe present-day sedimentation on the MRDF. Past findings indicate that sediment is initially deposited within ~30 km offshore of Southwest Pass and sediment focusing occurs proximal to Southwest Pass with respect to excess ^{234}Th (Corbett et al., 2004; Corbett et al., 2007). Other research in the Southwest Pass region indicates that the highest sediment deposition rates are observed proximal to the river outlet and SDRs show no correlation between morphological facies (Keller et al., 2017). The main objective of this research is to evaluate sedimentation rates and dispersal patterns of MR

sediment through the use of radiochemical tracers (^{7}Be and ^{234}Th) similar to studies done by Corbett et al., (2004), Corbett et al., (2007), and Keller et al., (2017). This study is a component of ongoing research that focuses on the temporal and spatial scales of submarine landslides and associated triggering mechanisms along the MRDF.

Chapter 2. Background

2.1. Study Area

The MRD is classified as a fluvial-dominated delta (Galloway, 1975; Walsh and Nittrouer, 2009), and the Mississippi River is the largest riverine system in North America with a drainage basin of 3.4 x 10^6 km^2 (Allison et al., 2012; Blum and Roberts, 2012). The study area of this research encompasses the MRDF along the Louisiana continental shelf offshore of the MR's major-first order distributaries, namely Southwest Pass (SW Pass), South Pass (S Pass), and Pass a Loutre (PAL) (Figure 2). The MR has an estimated annual sediment load ~ 210 Mt/yr, with fine silt and clay comprising ~ 80% of the total suspended load (Milliman and Meade, 1983). Core sites are located < 25 km from the mouth of the MR in water depths ranging between 27-258 m.

The delta front can be subdivided into four areas according to depth: interdistributary bays (0-10 m), upper delta front (10-70 m), intermediate delta front (70-120 m), and lower delta front (120-200 m) with each having common morphological features unique to their location (Coleman et al., 1998; Figure 3). Common features found in interdistributary bays include mud diapirs, collapse depressions (< 45 m in length), and bottleneck slides (< 610 m in length) (Coleman et al., 1980). Mudflow gullies are mainly found in areas ranging from interdistributary bays through the intermediate delta front and are the most dominant feature found throughout the MRDF. Gullies are typically tens kilometers in length and hundreds of meters in width with steep gradients flanking the edges up to 19° (Coleman et al., 1980). Gullies snake through the delta front and can often connect before transitioning to mudflow lobes in the lower delta front. Lobes serve as the primary location for sediment transported downslope from gullies and can often stack on another and intersect through time. Lobes vary in thickness, but are generally < 10

m thick. Core sampling for this study targeted four major facies, proximal and distal, along the MRDF, undisturbed seafloor (und), mudflow gully (gul), mudflow lobe (lob), and prodelta (pro).

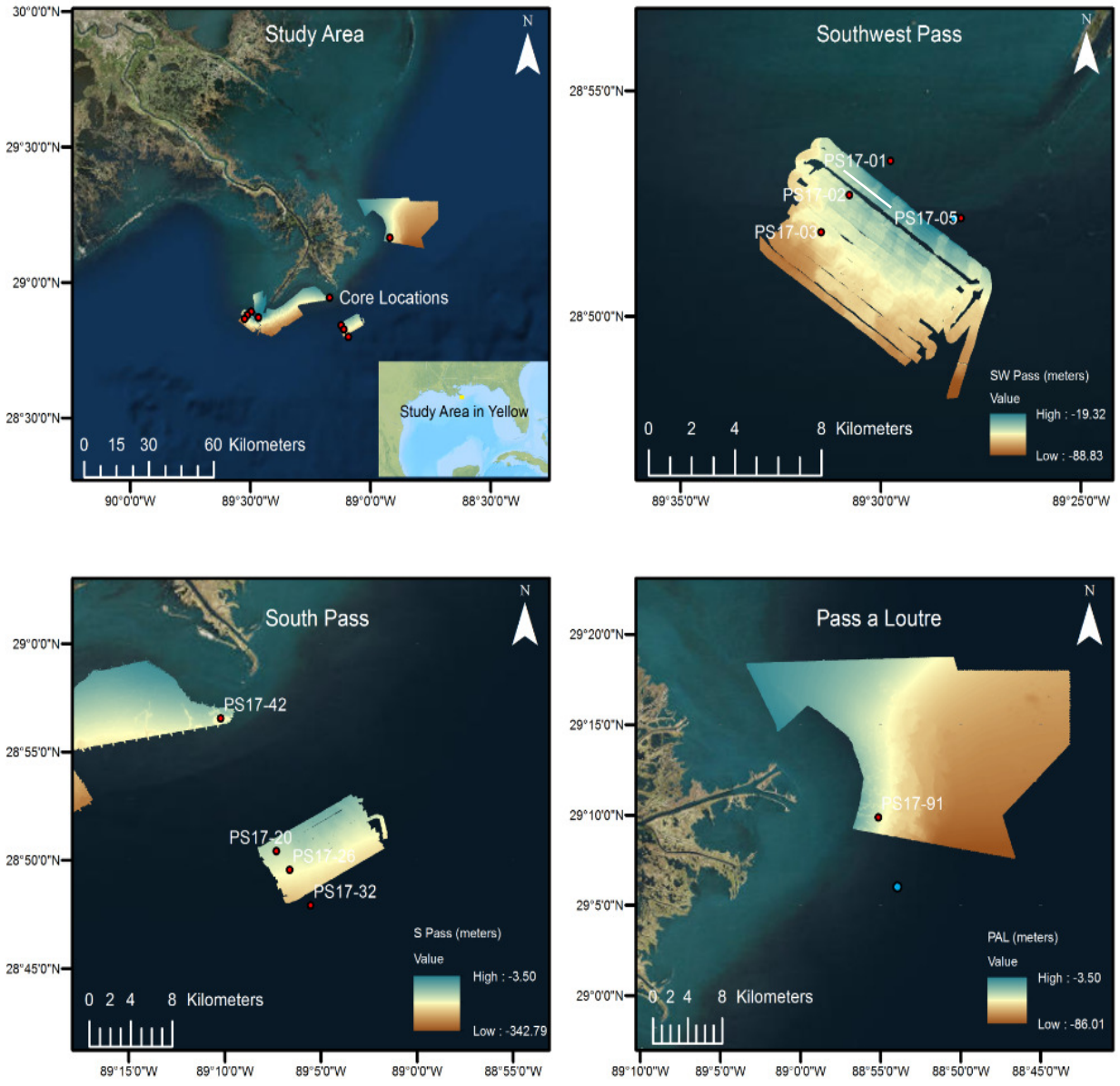

Figure 2. Field location. Map of study area and core sites (top left). Core locations denoted by red circles and CTD cast locations denoted by blue circles. CTD cast sites located only in Southwest Pass and Pass a Loutre study areas. Southwest Pass core sites (top right), white line depicts location of seismic line. South Pass core sites (bottom left). Pass a Loutre core sites (bottom right). Bathymetric data sourced from Baldwin et al., (2018).

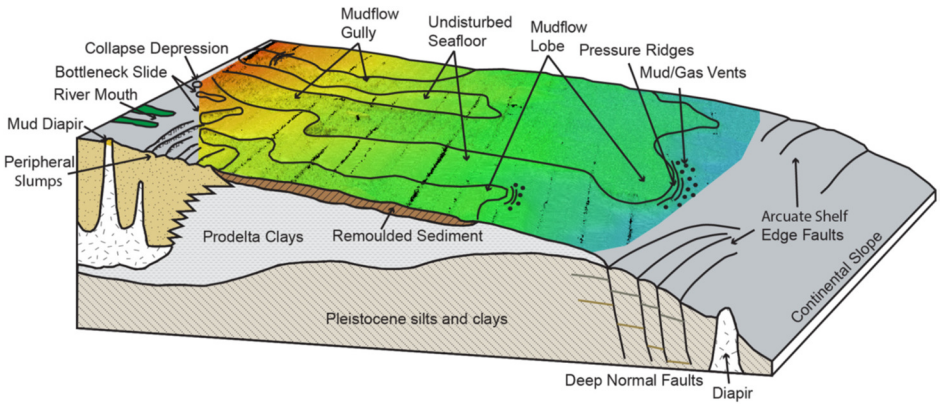

Figure 3. Common features on MRDF. Morphological features found along Mississippi River Delta Front as defined by Coleman et al., (1980), modified by Maloney et al., (2018). Rainbow bathymetry taken from Walsh et al., (2006) ranging from ~ 15 m in red to ~ 60 m in blue.

2.2. Evidence for Mass Failures and Triggering Mechanisms

Some of the earliest research extensively documenting mass failure events on the MRDF and their resulting morphological features have come from Coleman et al., (1980). Side-scan sonar, seismic imaging, and repeat bathymetric surveys were utilized by Coleman et al., (1980), in order to study slope failure events throughout the area. Morphological features, such as mudflow gullies and lobes, are produced from an interaction of high sediment input via the MR and slope failures. Mudflow gully and lobes on the MRDF are commonly found on the seafloor with slopes ranging between 0.5°-1.5° (Coleman et al., 1980), but slope failures have occurred in areas with a slope $< 0.3°$ (Bea, 1971).

Recent studies have used historic and new bathymetric data constructing difference-of-depth maps to evaluate vertical changes of the seafloor along the MRDF region to quantify areas of deposition and erosion (Obelcz et al., 2017; Maloney et al., 2018). Results from Maloney et al., (2018) highlighted mudflow lobe accretion and advancement in regions off SW Pass and S Pass with areas off PAL remaining quiescent. However, slope failures occurred in areas off PAL during the passage of Hurricane Rita (2004) and Katrina (2005) that took place after the recent

data sets used by Maloney et al., (2018), (Nodine et al., 2007). This suggests that areas along the MRDF offshore of all main passes experience mass failure events at varying temporal scales.

Mass movement of sediments downslope can be triggered from the following (Coleman, 1988):

1) Rapid sedimentation resulting in widespread loading

2) Coarse-grained sands and silts causing differential loading on underlying clays

3) Excess pore fluid pressures and low sediment strengths from rapid deposition of under consolidated fine-grained sediment

4) Large volumes of methane gas from degradation of organic material

5) Loading of seafloor from hurricanes and winter storms

Evidence for mass failures triggered by the passage of hurricanes on the MRDF has been studied largely in response to major infrastructure damage (Coleman et al., 1988; Nodine et al., 2007; Maloney et al., 2018). However, recent studies have shown the movement of sediment downslope during relatively quiescent periods suggesting that fair weather waves with an annual return may play a role as a triggering mechanism (Obelcz et al., 2017). Rapid sediment accumulation is considered to be a primary driver of mass failures on the MRDF (Coleman et al., 1988; Lee et al., 2007), but research has shown that mudflow lobe areas experience submarine mass wasting despite reduced sedimentation rates (Maloney et al., 2018), highlighting the need for more research focused on triggering mechanisms of failure events.

2.3. Changes in Sediment Load of Mississippi River

Human modification to the MR has resulted in a significant reduction in sediment load through time (Figure 4). The construction of dams, levee construction, sediment diversions, bank revetment, and better soil practices have all combined to the reduction of the MR's sediment

load. Dam construction throughout the MR drainage basin has reduced the sediment load by 50% (Blum and Roberts, 2009), with an estimated 40,000 dams constructed by the late 1990s (Bentley et al., 2016).

Early studies quantifying the total sediment load carried by the MR's major distributaries are as follows, SW Pass (145 Mt/yr), S Pass (90 Mt/yr), and PAL (185 Mt/yr) (Fisk et al., 1954). Later studies have shown a drastic reduction in sediment load and its distribution among the MR's distributaries. Average annual sediment loads calculated for water years 2008-2010 are as follows, SW Pass (20.8 Mt/yr), S Pass (4.7 Mt/yr), and PAL (4.8 Mt/yr) (Allison et al., 2012).

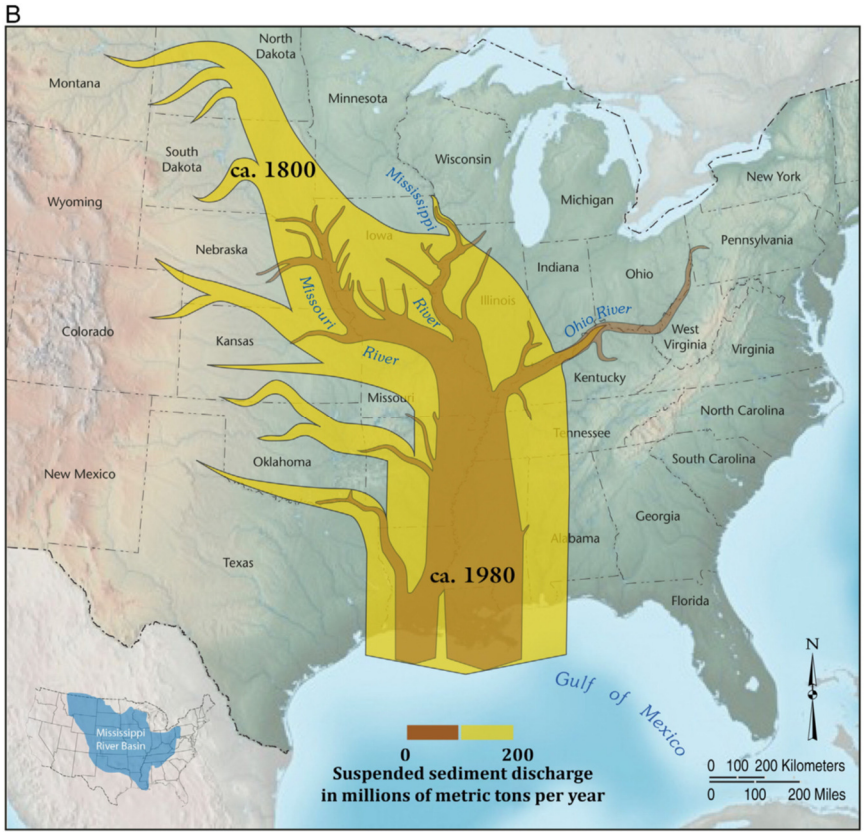

Figure 4. MR sediment load. Change in sediment load of the Mississippi River from 1800-1980 (Bentley et al., 2016).

This reduction in sediment load has caused the MRD to enter a state of degradation (Blum and Roberts, 2009; Maloney et al., 2018), likely has a significant impact on submarine mass movements on the MRDF, both spatially and temporally, but the long-term impacts are not yet

known. Changes in rates and patterns of sediment accumulation throughout the MRDF could affect stability and failure susceptibility of areas (Maloney et al., 2018). It is important to note that future sediment diversions along the MR (Mid-Barataria Bay; Mid-Breton Sound) will also reduce the amount of sediment reaching the delta front, possibly affecting the dynamics of submarine sedimentary processes on the MRDF. A reduction or increase of submarine landslides could be seen on the MRDF as a result of these changes.

Chapter 3. Methods

3.1. Field Work and Core Sampling/Processing

Field work was performed in early June 2017 aboard the *R/V Point Sur* offshore of the Mississippi River's main distributary outlets (SW Pass, S Pass, and PAL). Seafloor morphologies targeted for sampling ranged from undisturbed seafloor (und), mudflow gullies (gul), mudflow lobes (lob), and prodelta (pro). Prior to core collection, sampling locations were determined using recently collected multi-beam bathymetry and sub-bottom seismic data collected by USGS in May 2017 (Baldwin et al., 2018). Multicores were collected using a MC-800 multicore instrument manufactured by Ocean Instruments (10 cm diameter, 70 cm length). The MC-800 instrument collects eight replicate cores per deployment. (Figure 5).

Figure 5. Image of Ocean Instruments MC-800 multicore device. Credit- Andrew Courtois.

Following initial collection, a single core was chosen for radiochemical and grain-size analysis, a second core for X-radiography, and a third core to be archived for future studies. Cores restricted to radiochemical and grain-size analysis were extruded on deck and subsampled at 2-cm intervals. Core slabs for X-radiography (2 cm thick) were subsampled by inserting an open three-sided Plexiglass tray into the core tube then sealed by inserting a fourth side to prevent distortion of the sedimentary fabric (Bentley et al., 2003). Trays were fabricated prior to field collection.

3.2. Grain-size Analysis

Sediment samples for grain-size analysis were subsampled from multicores that were previously extruded on deck at 2 cm intervals. Wet sediment samples (< 1 mL) were placed in test tubes with 40 mL of a 0.05 % sodium phosphate solution to promote disaggregation. To account for organic material, a grain-size test was conducted that analyzed samples with organics present and removed that showed no major impact downcore on grain-size patterns. Prior to analysis, samples were vortexed and measured in a Beckham-Coulter laser diffraction particle analyzer (Model LS 13 320). Volume-frequency contour plots were generated for all cores using Sigmaplot© to graphically represent percent abundance of all grain sizes between 0.38 and 2,000 microns. A total number of 242 samples were analyzed for this study.

3.3. Radionuclide Analysis

Radionuclides of concern for this study include ^{7}Be (natural cosmogenic, $t_{1/2}$= 53.2 days) and ^{234}Th (natural ^{238}U series, $t_{1/2}$= 24.1 days). Samples were weighed and dried for 24 hours to determine water content, then ground up using a mortar and pestle and sealed into petri dishes. Canberra detectors (REGe, LEGe, and BEGe) were used for radionuclide measurement with single cores being restricted to one detector. Samples analyzed for ^{7}Be were counted within one

half-life from the date of collection. Associated activities of 477 keV and 63 keV were measured for detection of ^{7}Be and ^{234}Th. Sediment accumulation rates (SDR; cm/day) were calculated from both ^{7}Be and ^{234}Th using Equation 1 from Muhammed et al., (2008):

$$A_z = A_0 e^{(-\lambda z/S)}$$

where A_z is activity (dpm/g) at depth z (cm), A_0 is activity extrapolated to the surface (dpm/g), λ is the decay constant of ^{7}Be (0.01305 day^{-1}) or ^{234}Th (0.02876 day^{-1}), and S is the sediment deposition rate (cm/day). Inventories of ^{7}Be and ^{234}Th were calculated using Equation 2 from Muhammed et al., (2008):

$$I = \Sigma \rho_s \Delta z (1 - \Phi_i) A_i$$

where I is inventory (disintegrations per minute/centimeter^2, dpm/cm^2), ρ_s is mineral density (g/cm^3), Δz is the thickness of sample (2 cm), Φ_i is porosity calculated by water loss at 60 °C, and A_i is activity (dpm/g).

^{7}Be is produced naturally in the atmosphere from the bombardment of cosmic rays with nitrogen and oxygen atoms and is deposited from dry deposition and/or precipitation and absorbed onto sediments. It is often used as a tracer for fluvially-sourced sediments and a proxy for short-term sediment accumulation rates due to its relatively short half-life. (Corbett et al., 2004; Young, 2014; Keller et al., 2017; Restreppo et al., 2018). Natural background of ^{7}Be is considered to determine if core locations throughout the study area experience sediment focusing. Two regional studies of atmospheric deposition were used as a reference standard for annual theoretical ^{7}Be background (Baskaran et al. 1993, 14.7 dpm/cm^2; Corbett et al. 2004, 5.4 dpm/cm^2) to compare if sediment focusing occurred at core sites.

^{234}Th is continuously produced in marine waters from the decay of its parent, ^{238}U. Due to its short half-life and the restriction of ^{234}Th production in marine waters this study uses ^{234}Th

as a proxy for short-term sediment deposition rates and an indicator of resuspension events. Samples were initially analyzed for ^{234}Th and recounted after 6 months to quantify excess ^{234}Th, (total ^{234}Th activity - supported ^{234}Th activity). In order to calculate background ^{234}Th inventory, ^{238}U concentrations in the water column were calculated first. ^{238}U activities were derived from salinity measurements throughout the water column using Equation 3 from Owens et al., (2011):

$$^{238}U(\pm 0.047) = 0.0786 \times S - 0.315$$

where ^{238}U is measured in (dpm/cm^3) and S is salinity (ppt). Two locations (proximal to SW Pass sites; proximal to PAL site) were used for salinity data that was supplied from CTD casts in May 2017 in the study area. ^{234}Th flux was calculated using Equation 4 from Adhikari et al., (2016):

$$(F_{Th})_z = \lambda_{Th} \int (^{238}U - ^{234}Th)dz$$

where ^{238}U and ^{234}Th are the total water column activities of ^{238}U and ^{234}Th (dpm/cm^3), λ_{Th} is the radioactive decay constant for ^{234}Th, and $(F_{Th})_z$ is the integrated water column flux (dpm/cm^2 per day) of ^{234}Th at depth 'z' (m). For this study, a key assumption is that ^{238}U production in the water column is equal to ^{234}Th production, based on secular equilibrium. Therefore, ^{234}Th water column activity in Eqn. 4 will be effectively zero. A theoretical background ^{234}Th inventory was calculated using Equation 5 from Muhammed et al., (2008):

$$F = \lambda I$$

Where F is ^{234}Th flux in the water column (dpm/cm^2 per day), λ is ^{234}Th decay constant (0.02876 day^{-1}), and I is theoretical background ^{234}Th inventory (dpm/cm^2).

3.4. X-radiography

X-radiography was performed using a portable MinXray HF8015+dlp and Samsung Model SP501 detector panel. Image brightness/contrast was adjusted using ImageJ© and Adobe Illustrator©. Plots of bioturbation percentages down core were created through eye-observation

of X-radiograph images at 1 cm intervals. X-radiograph images of core slabs were overlain with a 1 cm grid and the percentage of bioturbation was recorded.

Chapter 4. Results

4.1. Grain-size Analysis

Grain-size analysis was performed by percent volume and displayed with frequency-contour plots. Plots are shown for cores located off SW Pass and S Pass (Figure 6-7).

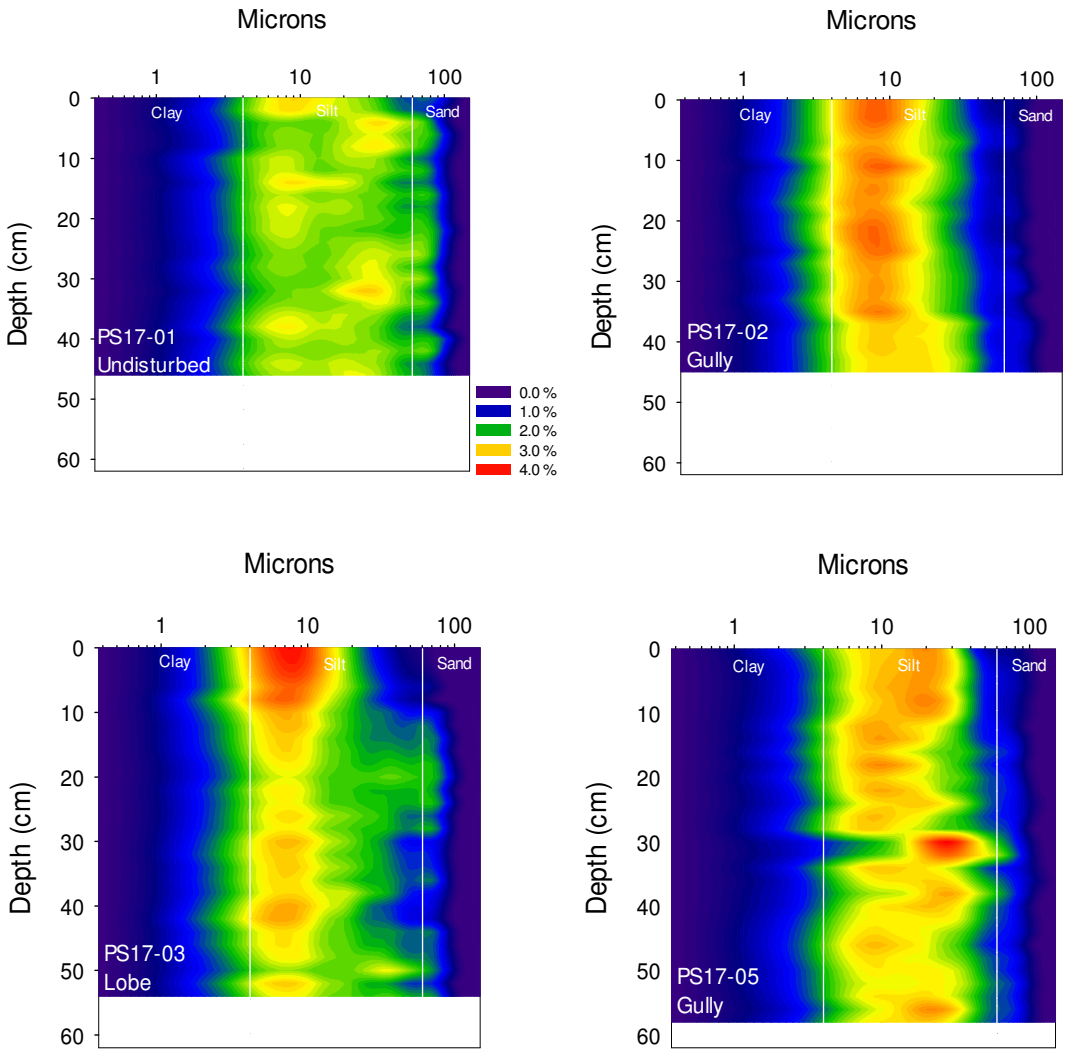

Figure 6. SW Pass grain-size plots. Southwest Pass grain-size plots by percent volume occurrence (0-4%). Clay, silt, and sand size ranges are denoted by vertical white lines.

Silt is the most common grain-size throughout the study area with cores ranging from ~ 66-73% silt by volume. On average, cores contain ~ 25% clay, ~ 69% silt, and ~ 6% sand, with a modal

grain size of very fine to fine silt. Downcore variations in modal grain size can be seen PS17-05 (30-35 cm) and PS17-32 (10-30 cm). Clay and sand content in cores ranges from ~ 20-32% and ~ 2-11%.

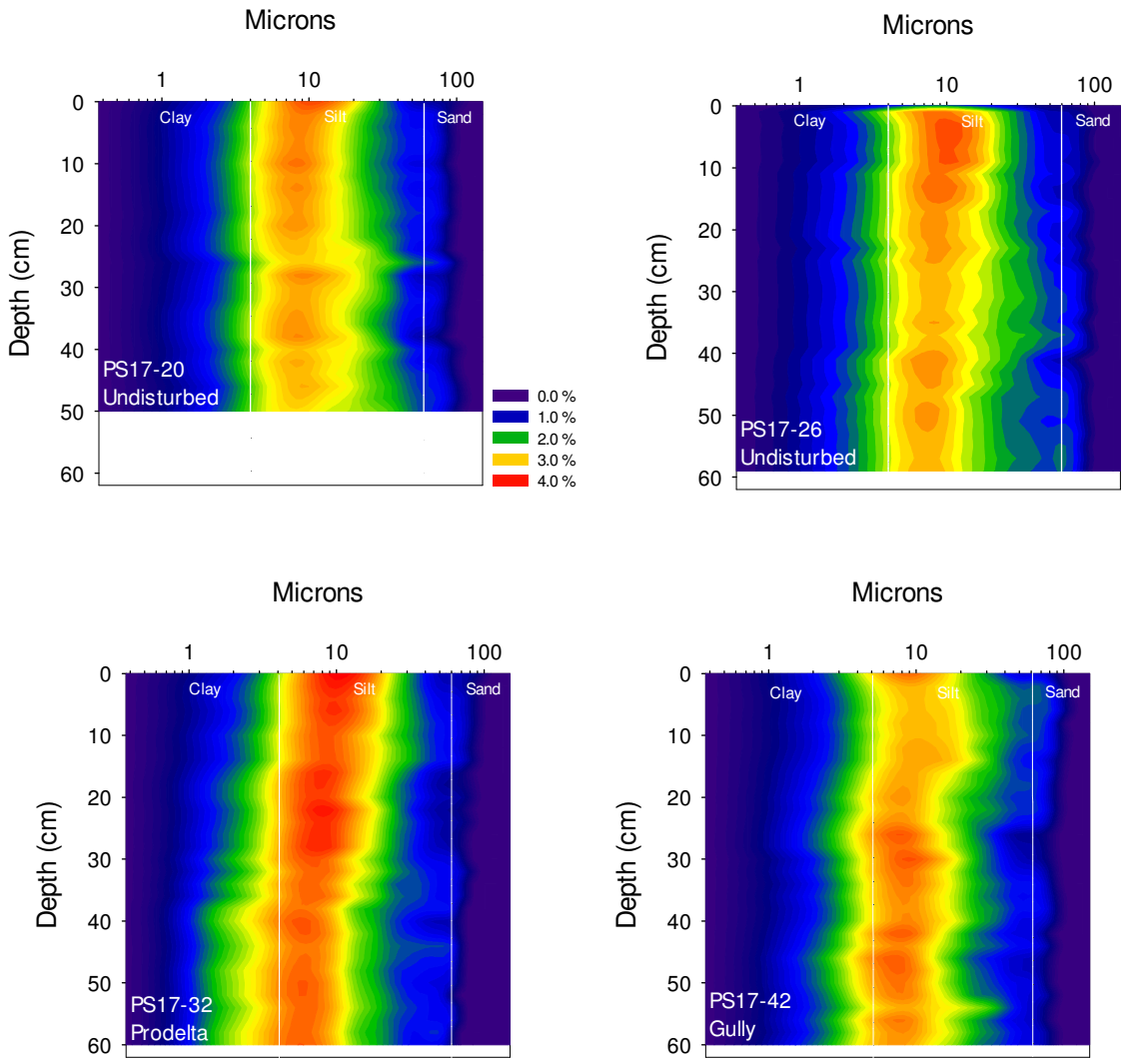

Figure 7. S Pass grain-size plots. South Pass grain-size plots by percent volume occurrence (0-4%). Clay, silt, and sand size ranges are denoted by vertical white lines.

Highest clay content occurs off S Pass (PS17-32), which is the deepest site (258 m) throughout the study area containing ~ 32% clay. Core locations in shallow water, proximal to the MR's main distributaries coincide with cores containing the greatest sand content, ranging ~ 7-11%.

4.2. Radionuclide Analysis

$^{234}Th_{xs}$ and ^{7}Be data are included in Tables 1-2. Four cores (PS17-02, PS17-03, PS17-05, and PS17-91) were analyzed for $^{234}Th_{xs}$ due to rapid ^{234}Th decay, in addition to ^{7}Be (Figure 8).

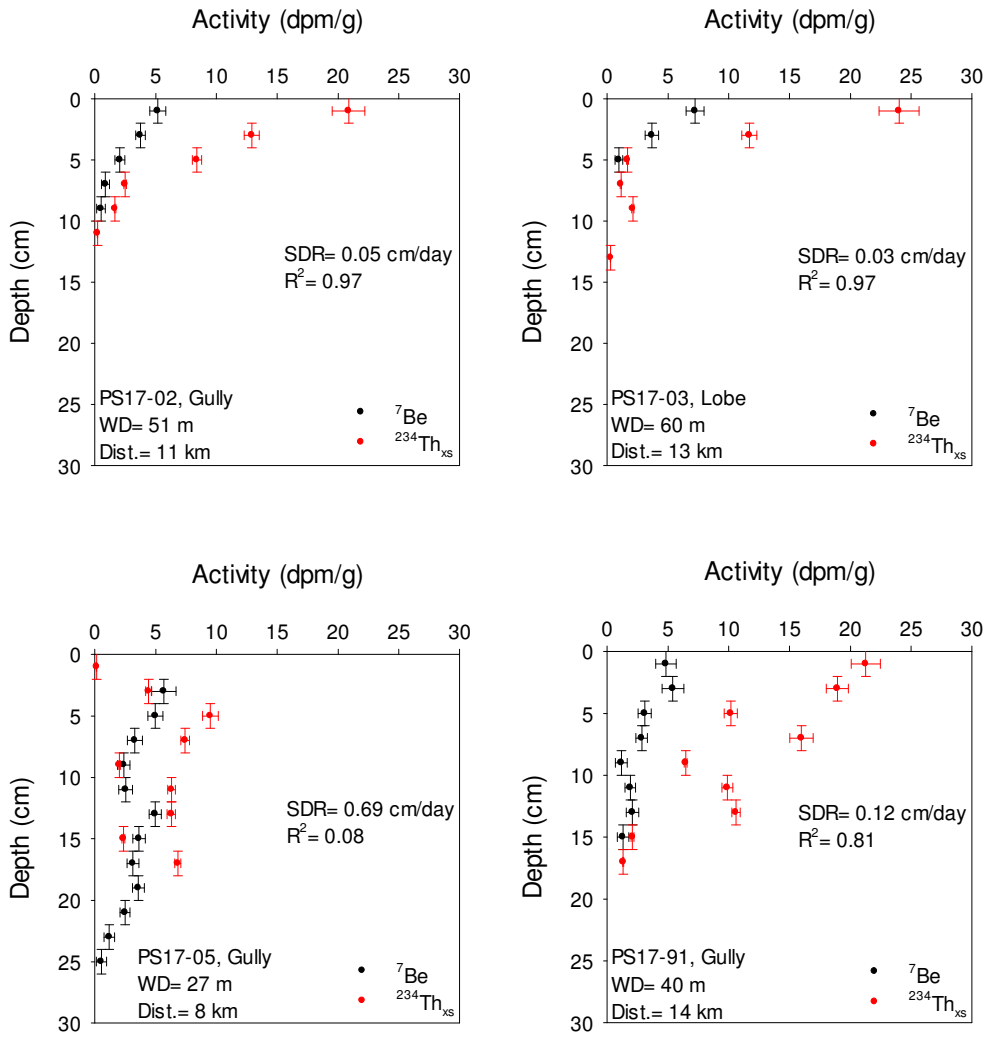

Figure 8. ^{7}Be and $^{234}Th_{xs}$ activity with depth. PS17-02, PS17-03, and PS17-05 are located off SW Pass and PS17-91 off S Pass. Water depth, distance from pass, and morphology denoted. SDR derived from Eqn. 1 (^{7}Be data). R^2 values reflect fit to Eqn. 1.

Surface activities and inventories of ^{7}Be and $^{234}Th_{xs}$ are plotted against water depth and distance from pass (see Appendix). Core locations within 15 km of the MR and at water depths less than 60 m, on average, exhibit ^{7}Be surface activities of ~ 5 dpm/g with the exception of SW Pass site

PS17-05. South Pass sites (PS17-20 and PS17-26) exhibit ^{7}Be surface activities of ~ 1 dpm/g and are located in deeper water (>185 m) and farther from the MR (>18 km). Cores analyzed for $^{234}Th_{xs}$ are all located within 15 km from the MR and lie in waters shallower than 41 m. ^{7}Be was detected in 8 out of 9 core locations (Figures 9-10). ^{7}Be was not detected at site PS17-32, which is the most distal core location in the study area, located approximately 23 km from S Pass at 258 m water depth. Mudflow gully core locations off of all the MR's main distributaries (SW Pass, S Pass, and PAL) exhibited the highest level of inventories, penetration depth, and SDRs in regards to ^{7}Be. These locations are less than 15 km from the nearest dominant river outlet and at water depths less than ~ 41 m.

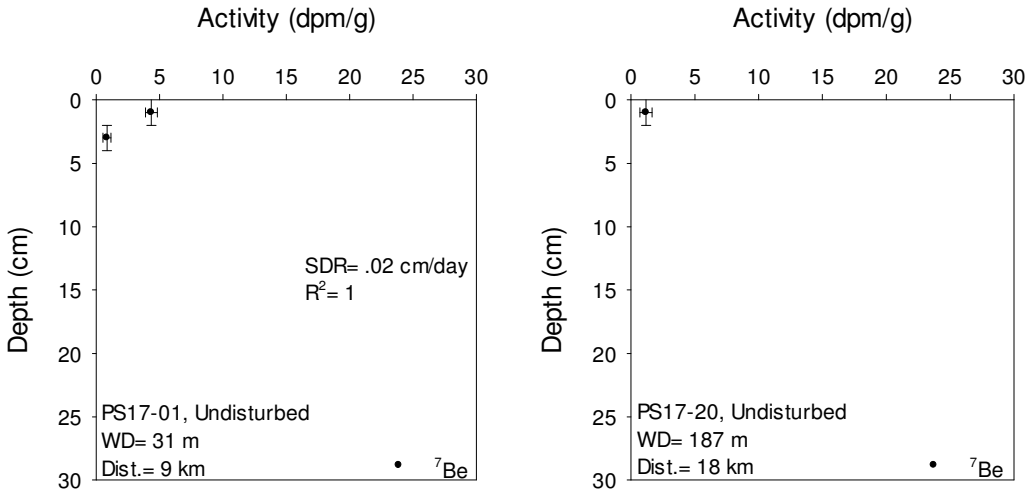

Figure 9. ^{7}Be activity with depth (SW and S Pass). PS17-01 located off SW Pass and PS17-20 located off S Pass. Water depth, distance from pass, and morphology denoted. SDR derived from Eqn. 1 (^{7}Be data). R^2 values reflect fit to Eqn. 1.

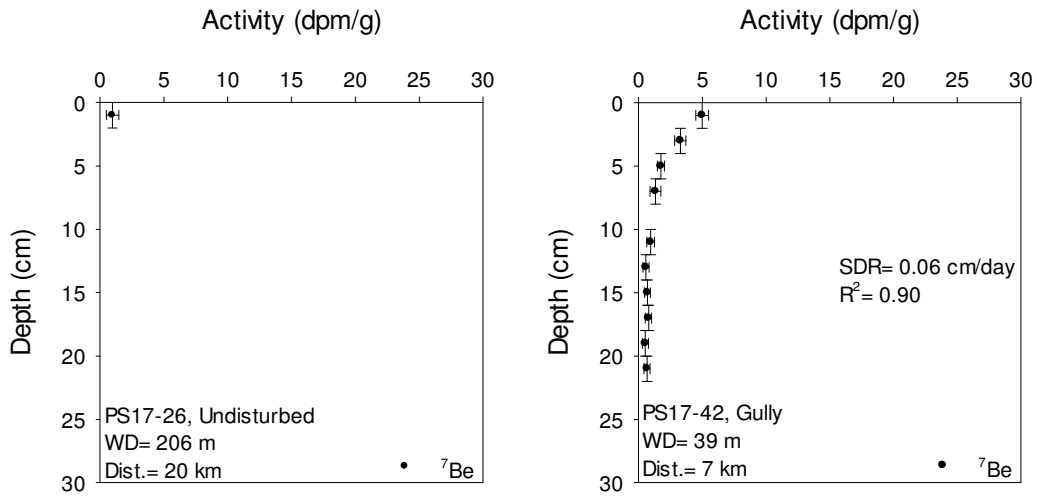

Figure 10. ^{7}Be activity with depth (S Pass). PS17-26, and PS17-42 are located off S Pass. Water depth, distance from pass, and morphology denoted.SDR derived from Eqn. 1 (^{7}Be data). R^2 values reflect fit to Eqn. 1.

4.3. X-radiography

X-radiograph images were created for all cores with ^{7}Be and $^{234}Th_{xs}$ penetration depths. Core locations proximal to the river-mouth exhibit a higher percentage of bedding layers while a general trend can be observed that shows an increase in bioturbation as core locations move farther offshore from the MR's main outlets. Southwest Pass core stations (PS17-03, PS17-05) display this trend (Figure 11). Throughout the study area, core sites off S Pass (PS17-20, PS17-26, PS17-32, and PS17-42) occur farthest from the river-mouth and in the deepest water. X-radiograph images of core sites off S Pass display an increase of bioturbation offshore, while site PS17-42, proximal to S Pass, displays multiple bedding layers with less bioturbation (see Appendix). Plots of the percentage of bioturbation were made for all cores throughout the study area through eye-observation of X-radiograph images at 1 cm intervals (Figure 12).

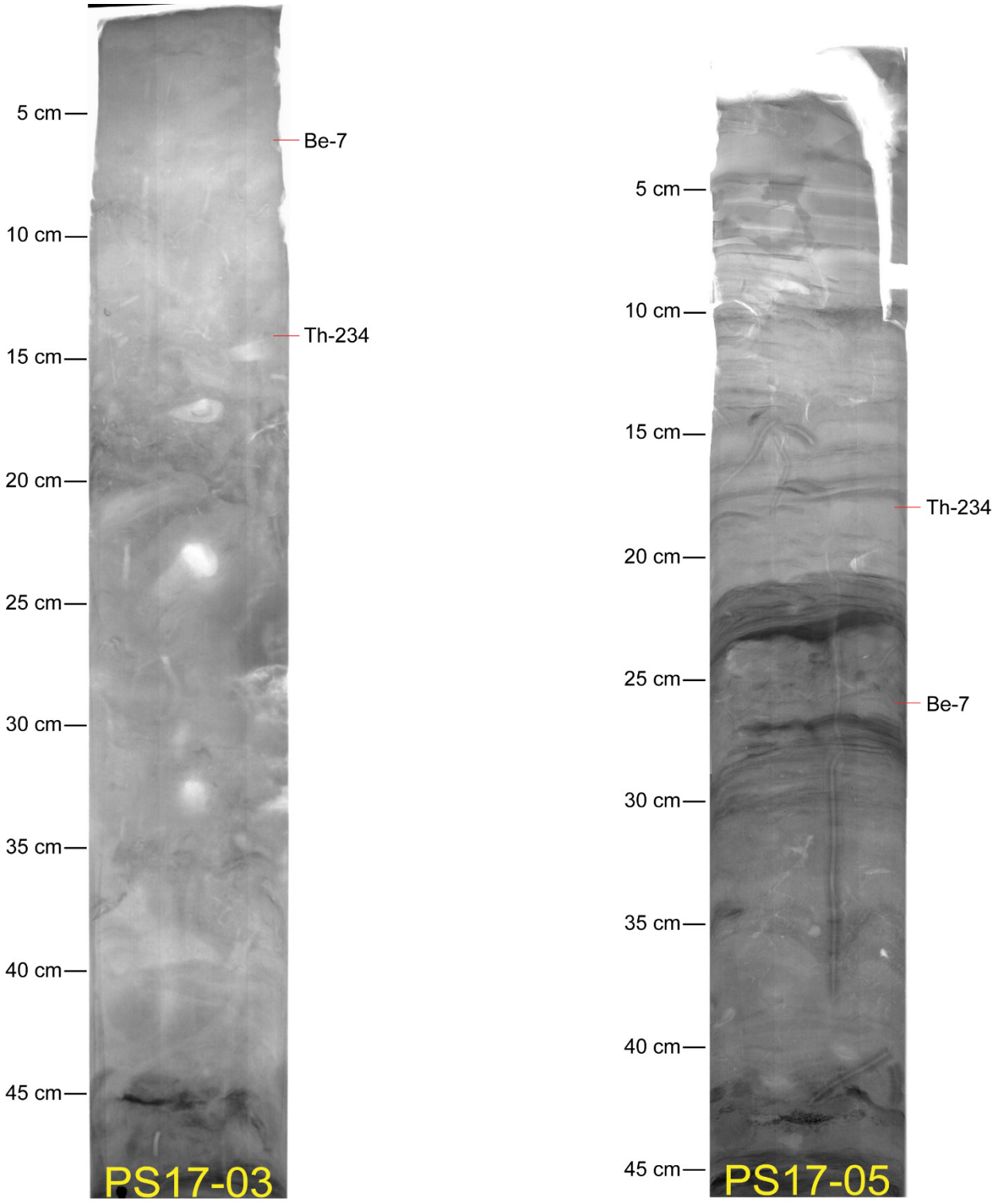

Figure 11. X-radiograph images of core locations off Southwest Pass. ^{7}Be and $^{234}Th_{xs}$ penetration depths labeled. Depth (cm) down core labeled at 5 cm intervals. Water depth for PS17-03 (lobe) is ~ 60 m and PS17-05 (gully) is ~ 27 m. Note increase in bioturbation from PS17-05 to PS17-03.

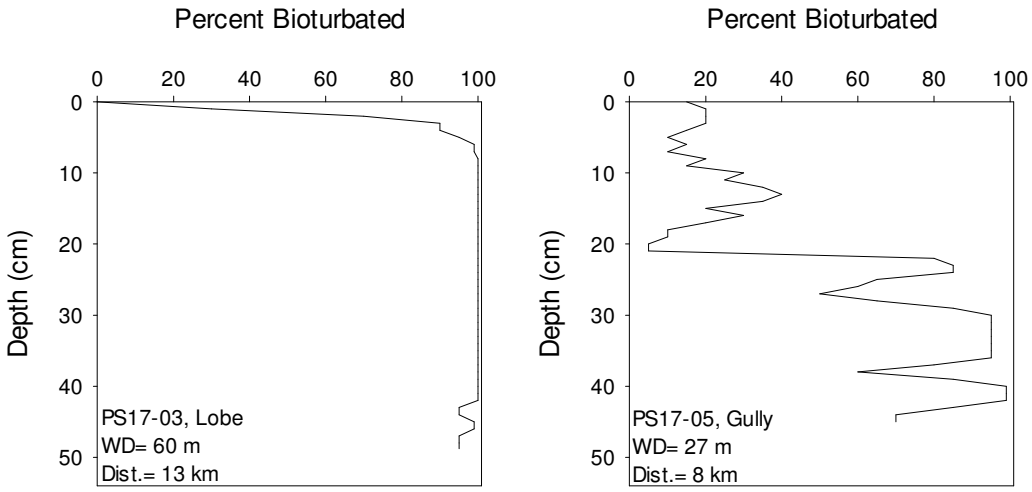

Figure 12. Plots of percentage of sedimentary fabric bioturbated of cores off SW Pass. Cores PS17-03 and PS17-05. Observations made at 1 cm intervals.

Table 1. Summary of excess ^{234}Th data.

Core ID	Water Depth (m)	Distance from Pass (km)	Facies	^{234}Th Theoretical Inventory (dpm/cm^2)	^{234}Th Core Inventory (dpm/cm^2)	$^{234}Th_{xs}$ Penetration Depth (cm)	$^{234}Th_{xs}$ SDR (cm/day)	SDR R^2
PS17-02	51	11	gul	5.78	33.70	12±1	0.1021±0.0109	0.98
PS17-03	60	13	lob	5.78	24.06	14±1	0.0640±0.0092	0.97
PS17-05	27	8	gul	5.78	44.42	18±1	N/A	N/A
PS17-91	14	14	gul	18.32	79.49	18±1	0.2774±0.0672	0.77

$^{234}Th_{xs}$ inventory derived from Eqn. 3 and Eqn. 4. $^{234}Th_{xs}$ SDR derived from Eqn. 1 and SDR R^2 reflects fit to Eqn. 1. Core sites PS17-02, PS17-03, and PS17-05 are located off SW Pass. Core site PS17-91 is located off PAL.

Table 2. Summary ^{7}Be data.

Core ID	Water Depth (m)	Distance from Pass (km)	Facies	^{7}Be Theoretical Inventory (dpm/cm^2)[a]	^{7}Be Theoretical Inventory (dpm/cm^2)[b]	^{7}Be Core Inventory (dpm/cm^2)	^{7}Be Penetration Depth (cm)	^{7}Be Surface Activity (dpm/g)	^{7}Be SDR (cm/day)[c]	SDR R^2
PS17-01	31	9	und	14.7	5.4	3.91	4±1	4.35	.0159	1
PS17-02	51	11	gul	14.7	5.4	9.15	10±1	5.17	0.0521±.0069	0.97
PS17-03	60	13	lob	14.7	5.4	6.62	6±1	7.22	0.0321±.0065	0.97
PS17-05	27	8	gul	14.7	5.4	37.56	26±1	N/D	0.6877±.7863	0.08
PS17-20	187	18	und	14.7	5.4	0.66	2±1	1.17	N/D	N/D
PS17-26	206	20	und	14.7	5.4	0.39	2±1	0.98	N/D	N/D
PS17-32	258	23	pro	14.7	5.4	N/D	N/D	N/D	N/D	N/D
PS17-42	39	7	gul	14.7	5.4	13.16	22±1	4.98	0.0601±.0096	0.90
PS17-91	40	14	gul	14.7	5.4	18.48	16±1	4.82	0.1221±.0267	0.81

Note- ^{7}Be background inventory[a] sourced from Baskaran et al., (1993) and ^{7}Be background inventory[b] sourced from Corbett et al., (2004). ^{7}Be SDR[c] derived from Eqn. 1 and SDR R^2 reflects fit to Eqn. 1. Core sites PS17-01, PS17-02, PS17-03, and PS17-05 located off Southwest Pass. Core sites PS17-20, PS17-26, PS17-32, and PS17-42 located off South Pass. Core site PS17-91 located off Pass a Loutre. N/D stands for “not detectable”.

Chapter 5. Discussion

Sediment transport via the MR is the primary transport mechanism along the MRDF. Past studies show that sediment deposition is concentrated within ~ 30 km of the river's main distributaries (Corbett et al., 2004; Xu et al., 2011; Keller et al., 2017). After initial deposition, waves, tides, currents, and sediment gravity-flows act as a transport mechanism redistributing sediment along the MRDF. Such transport can be observed cross-shelf or downslope. The series of mudflow gullies and lobes occurring on the MRDF are morphological features shaped by sediment transport from mass wasting events (Figure 1). A primary pathway for sediment transport downslope is from mudflow gullies to lobes (Figure 13).

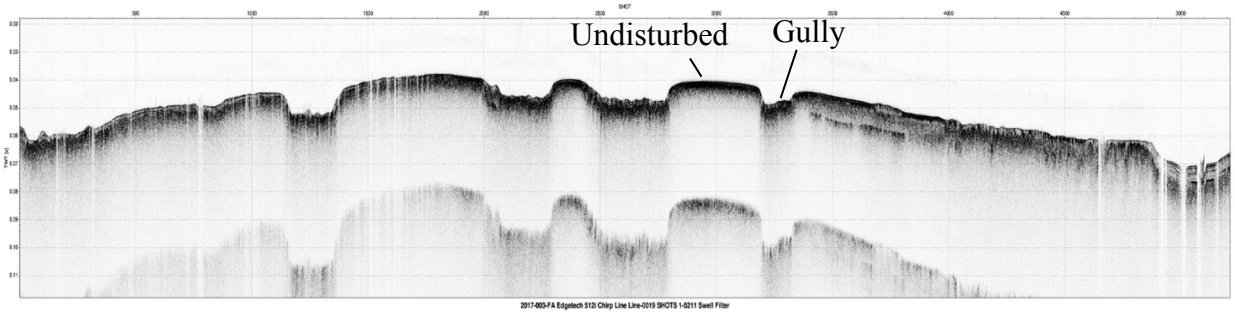

Figure 13. Seismic line of mudflow gullies and undisturbed seafloor along Southwest Pass. Mudflow gully labeled in image is associated gully upslope of station PS17-02. Shot number is shown on horizontal axis with two-way travel time (s) on vertical axis. Sourced from Baldwin et al., (2018).

Mudflow lobes are the main deposition center for sediment transported via mudflow gullies. Grain-size analysis from core locations off SW Pass (PS17-01, PS17-02, and PS17-03) may reflect the transport of sediment downslope. Core sites are located in a transect from shallow to deep water (PS17-01 at 31 m, PS17-02 at 51 m, and PS17-03 at 60 m). Grain-size analysis of cores shows PS17-01 having the highest percentage of sand, followed by PS17-03 and PS17-02 (Figure 6). It can be expected that locations proximal to the river contain coarser

grain-size due to settling velocities decreasing as the MR enters the Gulf of Mexico. The low occurrence of sand at PS17-02 and the appearance of sand down core in two intervals of PS17-03 may suggest the transport of material downslope from mudflow gullies to lobes. The two sandy intervals in PS17-03 were sieved to determine if grain-size analysis was skewed by organic material. A small percentage (< 5%) of foraminifera was observed, having negligible effects to grain-size results.

Radionuclide analysis of short-lived isotope ^{7}Be serves as a useful tracer of newly deposited material sourced from the MR and in determining short-term sediment deposition rates (Corbett et al., 2004; Keller et al., 2017; Restreppo et al., 2018). Due to its short half-life ($t_{1/2}$= 53.2 days), it is assumed that a major source for ^{7}Be is from sediment deposition from the MR prior to field collection (June 2017). A hydrograph of MR discharge from Tarbert Landing station shows that high discharge coincides with the timing of core collection (Figure 14).

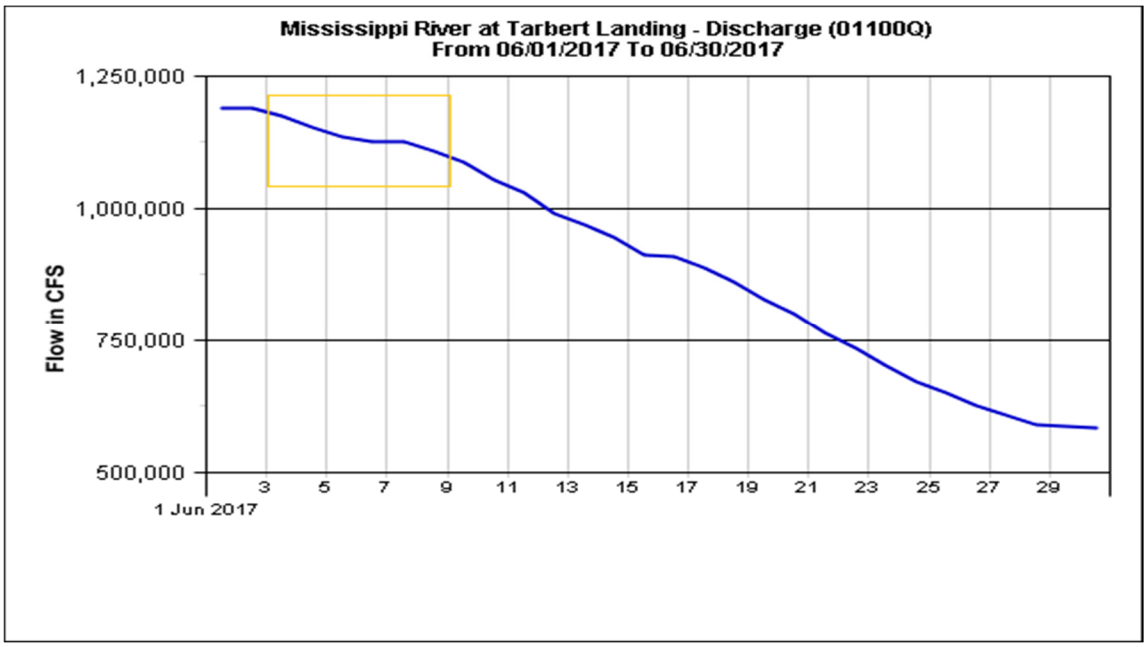

Figure 14. Hydrograph of Mississippi River discharge. June 1, 2017 to June 30, 2017 at Tarbert Landing (cubic feet per second). Orange box denotes dates of core collection. Source- USACE.

Areas of high sediment accumulation along the MRDF in this study correspond with the MR's dominant distributaries of sediment transport. Southwest Pass remains the dominant distributary of the MR transporting the majority of the sediment load and exhibiting the highest SDR throughout the MRDF (Allison et al., 2012). Cores analyzed for excess ^{234}Th inventory were greater than the calculated theoretical inventory, indicating that sediment focusing was taking place at these locations. SDRs calculated from excess ^{234}Th were approximately double than SDRs derived from ^{7}Be data. This can be attributed to the resuspension of sediment or sediment slowly descending through the water column prior to initial deposition. Generally, ^{7}Be inventories and penetration depths were highest throughout the SW Pass study site (Table 2). Pass a Loutre ranked second highest in ^{7}Be inventory followed by S Pass. Greatest ^{7}Be inventories and activities were seen within 30 km of the MR, coinciding with previous findings from Corbett et al., (2004), Keller et al., (2017), and Xu et al., (2011). Areas along the MRDF experiencing rapid sedimentation are prone to submarine landslide events (Coleman, 1988). Based on rapid sedimentation contributing to mass wasting events and that the highest ^{7}Be SDRs were observed off SW Pass possibly make this area more susceptible to mass failures compared to S Pass and PAL.

Out of the seafloor morphological facies sampled (undisturbed seafloor, mudflow gully, mudflow lobe, and prodelta), mudflow gullies throughout the MRDF recorded the highest SDRs, inventories, and penetration depths derived from ^{7}Be data (Table 1). It is important to note that only one SDR from an undisturbed seafloor location was able to be calculated (PS17-01). Two other undisturbed seafloor core sites (PS17-20, PS17-26) only exhibited ^{7}Be activity to a depth of 2 cm, in which a SDR was unable to be derived. To determine if sediment focusing took place at core locations, theoretical ^{7}Be inventory was taken in to account. For comparison, two studies,

with field locations similar in latitude to the MRDF, were used for a theoretical ^{7}Be inventory. Baskaran et al., (1993) measured a mean annual ^{7}Be inventory of 14.7 dpm/cm^{2} from Galveston Bay, TX. Corbett et al., (2004) used unpublished findings from McKee that measured a mean annual theoretical ^{7}Be inventory of 5.4 dpm/cm^{2} from Barataria Bay, LA. Two mudflow gully locations (PS17-05, SW Pass; PS17-91, PAL), exhibited higher ^{7}Be inventories than the inventory calculated by Baskaran et al., (1993). Three additional sites, (PS17-02 and PS17-03, SW Pass; PS17-42, S Pass), to those two previously mentioned, exhibited higher ^{7}Be inventories than the inventory used by Corbett et al., (2004). These findings indicate that seafloor morphologies of mudflow gullies and mudflow lobes experience sediment focusing. Possible scenarios for sediment focusing at mudflow gullies and lobes are as follows:

1) Gullies and lobes receive more sediment because gravity flows develop as sediment is depositing.

2) Wave-enhanced sediment-gravity flows (WESGFs) occur with resuspension of river-borne sediment (Macquaker et al., 2010; Denommee et al., 2016; Denommee et al., 2018).

3) Resuspension of sediment from undisturbed seafloor and ridges, due to higher bed-shear stresses from waves compared to gullies and lobes that are located in deeper water.

It is important to determine if distance of core sites from the river-mouth is a primary control on sediment focusing. Southwest Pass core sites PS17-01 (und), PS17-02 (gul), and PS17-03 (lob) are arranged in a transect and effectively capture what effect distance from the river-mouth has on sediment deposition (Figure 2). ^{7}Be core inventory, penetration depth, and SDR for site PS17-01, located on undisturbed seafloor and proximal to SW Pass, are all lower than measurements recorded at sites PS17-02 and PS17-03, which are located farther offshore and in deeper water. In addition, site PS17-05 (gul) off SW Pass is located in a similar water depth and distance from

the river-mouth as site PS17-01, but registers significantly higher ^{7}Be inventory, SDR, and penetration depth. ^{7}Be inventories from cores located off SW Pass exhibit greater inventories than the theoretical inventory used by Corbett et al., (2004), with the exception of PS17-01. Cores PS17-42 off S Pass and PS17-91 off PAL are located at similar water depths (±1 m) and similar morphologies (mudflow gullies), but different distances from the river-mouth (PS17-42, 7 km; PS17-91, 14 km). Also, recent research has shown that the two distributaries, S Pass and PAL, have similar sediment discharges (Allison et al., 2012). These similarities between sites, with the primary difference being distance from the river-mouth, provide sufficient information to evaluate the possible controls on sediment focusing. It was found that both sites experience sediment focusing when compared to the theoretical inventory used by Corbett et al., (2004). However, PS17-91 (PAL) located 7 km farther offshore than PS17-42 (S Pass), exhibits a higher ^{7}Be inventory and SDR than PS17-42. ^{7}Be data from SW Pass cores and core sites located in gullies off S Pass and PAL indicate that other mechanisms, besides proximity to the river-mouth, primarily control sediment focusing of ^{7}Be laden sediment at locations with known morphologies of mudflow gullies and lobes. It is important to note that all ^{7}Be core inventories calculated from undisturbed seafloor locations observed lower inventories than both the theoretical inventories used from Baskaran et al., (1993) and Corbett et al., (2004). These findings indicate that sediment focusing is correlated with specific seafloor morphologies of mudflow gullies and mudflow lobes and that these morphologies are primary locations of sediment deposition along the MRDF.

Wave and/or current influence on the seafloor is evident in X-radiographic images of PS17-91, off PAL, where cross-bedding is present. (Figure 15). X-radiograph images throughout the rest of the study area only exhibit planar bedding features, a source of hemi-pelagic

deposition. The findings of excess ^{234}Th inventories greater than the calculated ^{234}Th theoretical inventory combined with the presence of cross-bedding suggest that waves and/or currents have a strong influence across the MRDF, specifically at core site PS17-91.

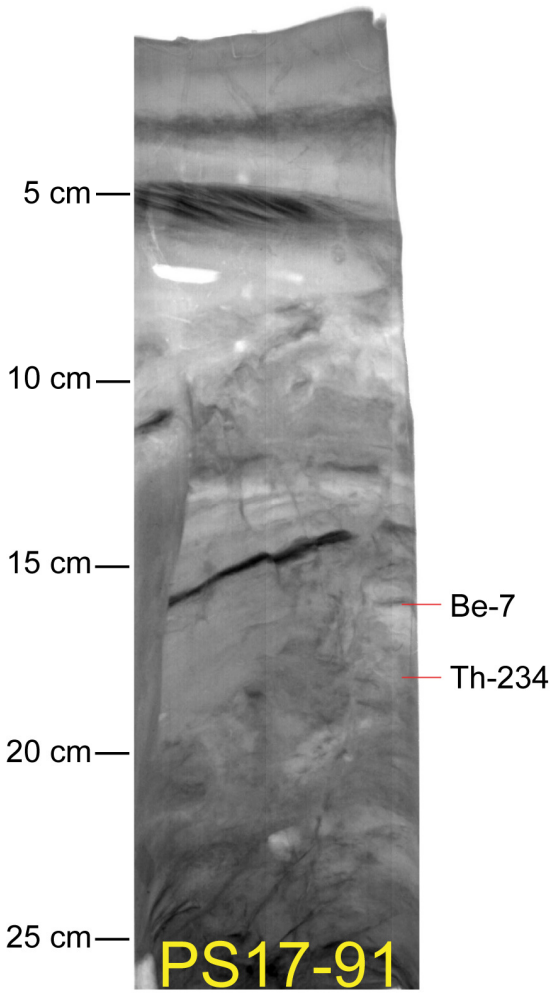

Figure 15. X-radiograph image of PS17-91. Core located off Pass a Loutre in a mudflow gully. Cross-bedding occurs ~ 5 cm downcore. ^{7}Be and $^{234}Th_{xs}$ penetration depths labeled.

It is noted that currents play an important role in the transportation of sediment, however river flow and waves are the main influences on the deposition and resuspension of fluvial and marine sediments on the Louisiana shelf (Corbett et al., 2007). X-radiography of core sites throughout the study region show a general trend of increasing bioturbation as water depth and distance from the MR increases. Core sites proximal to the river-mouth experience high SDR, increased

presence of bedding, and low bioturbation in comparison to core sites located farther offshore, that exhibit high rates of bioturbation. Bioturbation plots and X-radiograph images of cores taken off SW Pass and S Pass display this relationship (Figures 14-17). This is directly related to the preservation potential of sedimentary event layers (Wheatcroft, 1990; Bentley et al., 2006). Core locations proximal to the MR have a higher preservation potential compared to distal sites. X-radiograph images show the relationship that the biogenic sedimentary fabric is likely to overprint the sedimentary fabric in sediments when the rate of bioturbation significantly exceeds the net combined rates of physical reworking and deposition (Bentley et al., 2006).

Chapter 6. Conclusions

This research provides a regional survey of active sediment deposition throughout the MRDF through the use of short-lived radioisotopes. Understanding processes such as sedimentation is an important component in determining what areas of the MRDF are prone to submarine landslides. Historic changes to the sediment load of the MR and sediment dispersal patterns along the MRDF have strong influences on submarine landslide temporally and spatially, highlighting the significance of this study. The following are the significant findings of this study:

1) Despite substantial reductions of the MR sediment load, ^{7}Be analysis shows active sediment deposition of fluvially sourced sediment offshore from all major outlets.

2) ^{7}Be analysis shows that core sites received the greatest amount of sediment proximal to the river-mouth, decreasing offshore. SW Pass experienced the highest sediment deposition rates (0.2 cm/day on average), followed by PAL and S Pass.

3) Mudflow gully locations exhibit the highest sediment deposition rates, derived from ^{7}Be analysis, out of all facies targeted (undisturbed seafloor, mudflow gully, mudflow lobe, prodelta) across the entire sampling area.

4) Sediment focusing was determined at 5 core locations (1 lobe and 2 gully sites off SW Pass; 1 gully site off S Pass; 1 gully site off PAL) based on theoretical ^{7}Be inventories used by Corbett et al., (2004). Sediment focusing was determined at a gully located off SW Pass and a gully located off PAL based on theoretical ^{7}Be inventories used by Baskaran et al., (1993).

5) Sediment deposition rates determined from excess ^{234}Th for sites PS17-02, PS17-03, and PS17-91 were double than those determined from ^{7}Be, suggesting a strong influence from waves and/or currents on the redistribution of sediment.

6) X-radiograph analysis of cores show a general trend of increasing bioturbation present as distance offshore increases, with core sites proximal to the river-mouth more likely to preserve bedding layers.

Based on the direct relationship between the sediment load of the MR and sediment deposition on the delta front, future surveys should be considered in light of coastal restoration efforts using the MR for proposed sediment diversions. A loss of sediment to the MRDF through sediment diversions will likely have an impact on the occurrence of submarine landslides in the region.

References

Adhikari, P.L., Maiti, K., Overton, E.B., Rosenheim, B.E. and Marx, B.D., 2016. Distributions and accumulation rates of polycyclic aromatic hydrocarbons in the northern Gulf of Mexico sediments. *Environmental pollution*, *212*, pp.413-423.

Allison, M.A., Demas, C.R., Ebersole, B.A., Kleiss, B.A., Little, C.D., Meselhe, E.A., Powell, N.J., Pratt, T.C. and Vosburg, B.M., 2012. A water and sediment budget for the lower Mississippi–Atchafalaya River in flood years 2008–2010: implications for sediment discharge to the oceans and coastal restoration in Louisiana. *Journal of Hydrology*, *432*, pp.84-97.

Baldwin, W.E., Ackerman, S.D., Worley, C.R., Danforth, W.W., and Chaytor, J.D, 2018, High-resolution geophysical data collected along the Mississippi River Delta front offshore of southeastern Louisiana, U.S. Geological Survey Field Activity 2017-003-FA: U.S. Geological Survey data release, https://doi.org/10.5066/F7X929K6.

Baskaran, M., Coleman, C.H. and Santschi, P.H., 1993. Atmospheric depositional fluxes of 7Be and 210Pb at Galveston and College Station, Texas. *Journal of Geophysical Research: Atmospheres*, *98*(D11), pp.20555-20571.

Bea, R.G., 1971. How sea floor slides affect offshore structures. *Oil and Gas Journal*, *69*(48), pp.88-92..

Bentley, S.J. and Nittrouer, C.A., 2003. Emplacement, modification, and preservation of event strata on a flood-dominated continental shelf: Eel shelf, Northern California. *Continental Shelf Research*, *23*(16), pp.1465-1493.

Bentley, S.J., Sheremet, A. and Jaeger, J.M., 2006. Event sedimentation, bioturbation, and preserved sedimentary fabric: field and model comparisons in three contrasting marine settings. *Continental Shelf Research*, *26*(17-18), pp.2108-2124.

Bentley, S.J., Blum, M.D., Maloney, J., Pond, L. and Paulsell, R., 2016. The Mississippi River source-to-sink system: Perspectives on tectonic, climatic, and anthropogenic influences, Miocene to Anthropocene. *Earth-Science Reviews*, *153*, pp.139-174.

Blum, M.D. and Roberts, H.H., 2009. Drowning of the Mississippi Delta due to insufficient sediment supply and global sea-level rise. *Nature Geoscience*, *2*(7), p.488.

Blum, M.D. and Roberts, H.H., 2012. The Mississippi delta region: past, present, and future. *Annual Review of Earth and Planetary Sciences*, *40*, pp.655-683.

Coleman, J. M., Prior, D. B., and Garrison, L. E., 1980, Subaqueous sediment instabilities in the offshore Mississippi River delta: U.S. Department of the Interior, Bureau of Land Management.

Coleman, J.M., 1988. Dynamic changes and processes in the Mississippi River delta. *Geological Society of America Bulletin*, *100*(7), pp.999-1015.

Coleman, J.M., Roberts, H.H. and Stone, G.W., 1998. Mississippi River delta: an overview. *Journal of Coastal Research*, pp.699-716.

Coleman, J.M., Suhayda, J.N., Whelan, T. and Wright, L.D., 1974. Mass movement of Mississippi River delta sediments.

Corbett, D.R., McKee, B. and Duncan, D., 2004. An evaluation of mobile mud dynamics in the Mississippi River deltaic region. *Marine Geology*, *209*(1-4), pp.91-112.

Corbett, D.R., Dail, M. and McKee, B., 2007. High-frequency time-series of the dynamic sedimentation processes on the western shelf of the Mississippi River Delta. *Continental Shelf Research*, *27*(10-11), pp.1600-1615.

Denommee, K.C., Bentley, S.J. and Harazim, D., 2018. Mechanisms of muddy clinothem progradation on the Southwest Louisiana Chenier Plain inner shelf. *Geo-Marine Letters*, *38*(3), pp.273-285.

Denommee, K.C., Bentley, S.J., Harazim, D. and Macquaker, J.H., 2016. Hydrodynamic controls on muddy sedimentary-fabric development on the Southwest Louisiana subaqueous delta. *Marine Geology*, *382*, pp.162-175.

Fisk, H.N., Kolb, C.R., McFarlan, E. and Wilbert, L.J., 1954. Sedimentary framework of the modern Mississippi delta [Louisiana]. *Journal of Sedimentary Research*, *24*(2), pp.76-99.

Galloway, W.E., 1975. Process framework for describing the morphologic and stratigraphic evolution of deltaic depositional systems.

Hitchcock, C., Givler, R., Angell, M. and Hooper, J., 2010. GIS-based assessment of submarine mudflow hazard offshore of the Mississippi Delta, Gulf of Mexico. In *Submarine Mass Movements and Their Consequences* (pp. 353-364). Springer, Dordrecht.

Keller, G., Bentley, S.J., Georgiou, I.Y., Maloney, J., Miner, M.D. and Xu, K., 2017. River-plume sedimentation and 210 Pb/7 Be seabed delivery on the Mississippi River delta front. *Geo-Marine Letters*, *37*(3), pp.259-272.

Lee, H.J., Locat, J., Desgagnés, P., Parsons, J.D., McAdoo, B.G., Orange, D.L., Puig, P., Wong, F.L., Dartnell, P. and Boulanger, E., 2007. Submarine mass movements on continental margins. In *Continental margin sedimentation: from sediment transport to sequence stratigraphy* (Vol. 37, pp. 213-274). Blackwell Publishing.

Macquaker, J.H., Bentley, S.J. and Bohacs, K.M., 2010. Wave-enhanced sediment-gravity flows and mud dispersal across continental shelves: Reappraising sediment transport processes operating in ancient mudstone successions. *Geology*, *38*(10), pp.947-950.

Maloney, J.M., Bentley, S.J., Xu, K., Obelcz, J., Georgiou, I.Y. and Miner, M.D., 2018. Mississippi River subaqueous delta is entering a stage of retrogradation. *Marine Geology*, *400*, pp.12-23.

Milliman, J.D. and Meade, R.H., 1983. World-wide delivery of river sediment to the oceans. *The Journal of Geology*, *91*(1), pp.1-21.

Muhammad, Z., Bentley, S.J., Febo, L.A., Droxler, A.W., Dickens, G.R., Peterson, L.C. and Opdyke, B.N., 2008. Excess 210Pb inventories and fluxes along the continental slope and basins of the Gulf of Papua. *Journal of Geophysical Research: Earth Surface*, *113*(F1).

Nodine, M.C., Cheon, J.Y., Wright, S.G. and Gilbert, R.B., 2007. Mudslides during Hurricane Ivan and an Assessment of the Potential for Future Mudslides in the Gulf of Mexico. *MMS Project*, (552).

Obelcz, J., Xu, K., Georgiou, I.Y., Maloney, J., Bentley, S.J. and Miner, M.D., 2017. Sub-decadal submarine landslides are important drivers of deltaic sediment flux: Insights from the Mississippi River Delta Front. *Geology*, *45*(8), pp.703-706.

Owens, S.A., Buesseler, K.O. and Sims, K.W.W., 2011. Re-evaluating the 238U-salinity relationship in seawater: Implications for the 238U–234Th disequilibrium method. *Marine Chemistry*, *127*(1-4), pp.31-39.

Prior, D.B. and Suhayda, J.N., 1979, January. Submarine mudslide morphology and development mechanisms, Mississippi Delta. In *Offshore Technology Conference*. Offshore Technology Conference.

Restreppo, G.A., Bentley, S.J., Wang, J. and Xu, K., 2018. Riverine Sediment Contribution to Distal Deltaic Wetlands: Fourleague Bay, LA. *Estuaries and Coasts*, pp.1-13.

Walsh, J.P., Corbett, R., Mallinson, D., Goni, M., Dail, M., Loewy, C., Marciniak, K., Ryan, K., Smith, C., Stevens, A. and Summers, B., 2006. Mississippi delta mudflow activity and 2005 Gulf hurricanes. *Eos, Transactions American Geophysical Union*, *87*(44), pp.477-478.

Walsh, J.P. and Nittrouer, C.A., 2009. Understanding fine-grained river-sediment dispersal on continental margins. *Marine Geology*, *263*(1-4), pp.34-45.

Wheatcroft, R.A., 1990. Preservation potential of sedimentary event layers. *Geology*, *18*(9), pp.843-845.

Xu, K., Harris, C.K., Hetland, R.D. and Kaihatu, J.M., 2011. Dispersal of Mississippi and Atchafalaya sediment on the Texas–Louisiana shelf: Model estimates for the year 1993. *Continental Shelf Research*, *31*(15), pp.1558-1575.

Young, D. R., 2014, Examination of the 2011 Mississippi River Flood Deposit on the Louisiana Continental ShelfMaster's Thesis]: East Carolina University.

Appendix. Additional Multicore Data

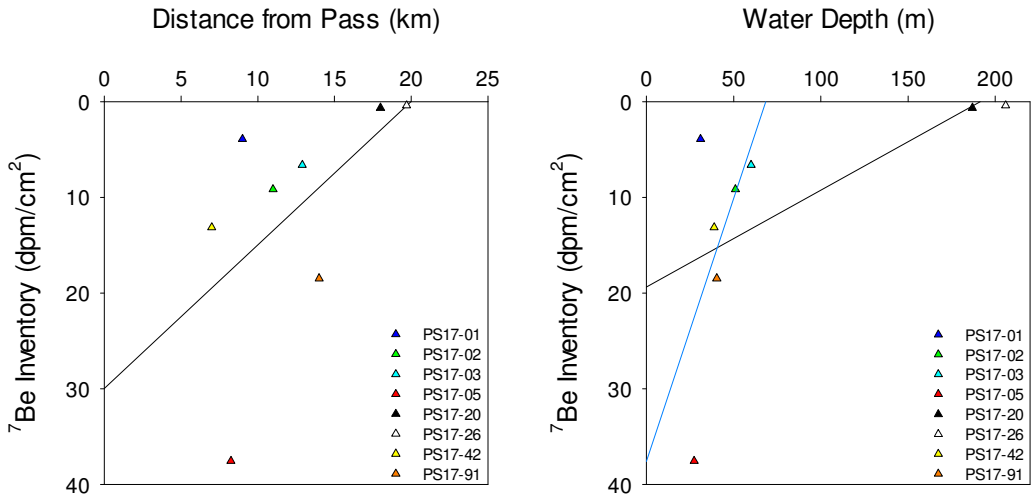

A1: ^{7}Be inventory (dpm/cm^{2}) versus distance from pass (km), R^2= 0.31 (left); and water depth (m), R^2= 0.36 (right; black line), R^2= 0.30 (right; blue line) for all cores except PS17-20 and PS17-26. Samples analyzed for ^{7}Be are denoted by triangles.

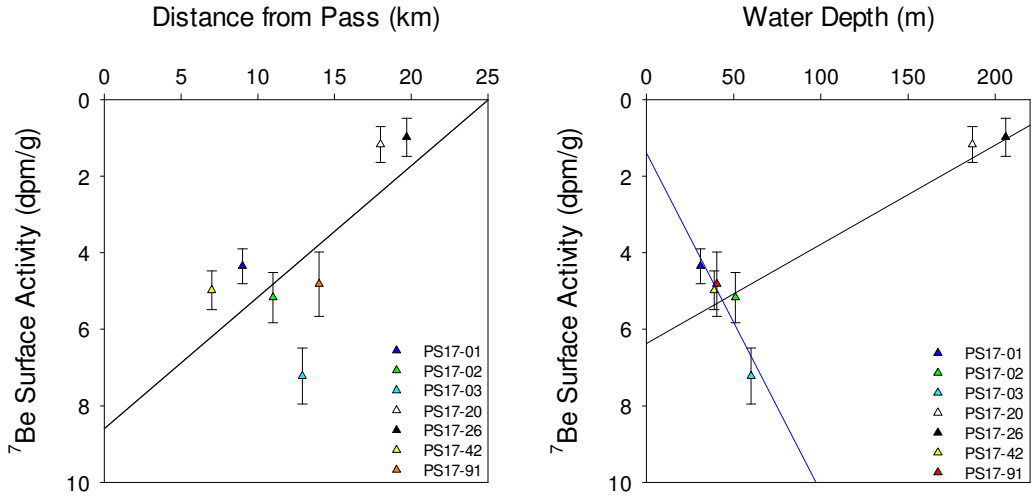

A2: ^{7}Be surface activity (dpm/g) versus distance from pass (km), R^2= 0.49 (left); and water depth (m), R^2= 0.74 (right; black line), R^2=0.82 (right; blue line) for cores PS17-01, PS17-02, PS17-03, PS17-42, and PS17-91. ^{7}Be surface activity was not detected in Core PS17-05, therefore it is not plotted. Samples analyzed for ^{7}Be are denoted by triangles.

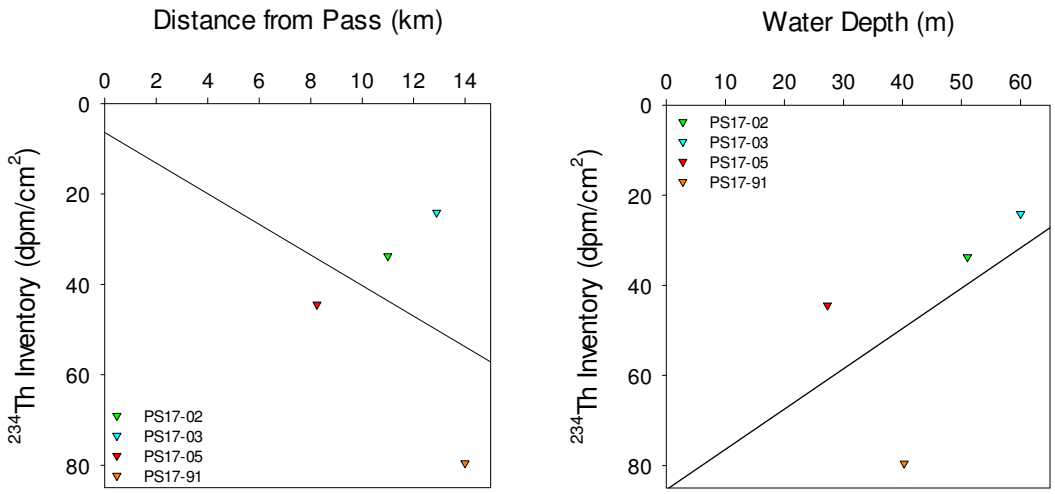

A3: Excess ^{234}Th inventory (dpm/cm^2) versus distance from pass (km), R^2= 0.12 (left); and water depth (m), R^2= 0.27 (right). Samples analyzed for ^{234}Th are denoted by upside down triangles.

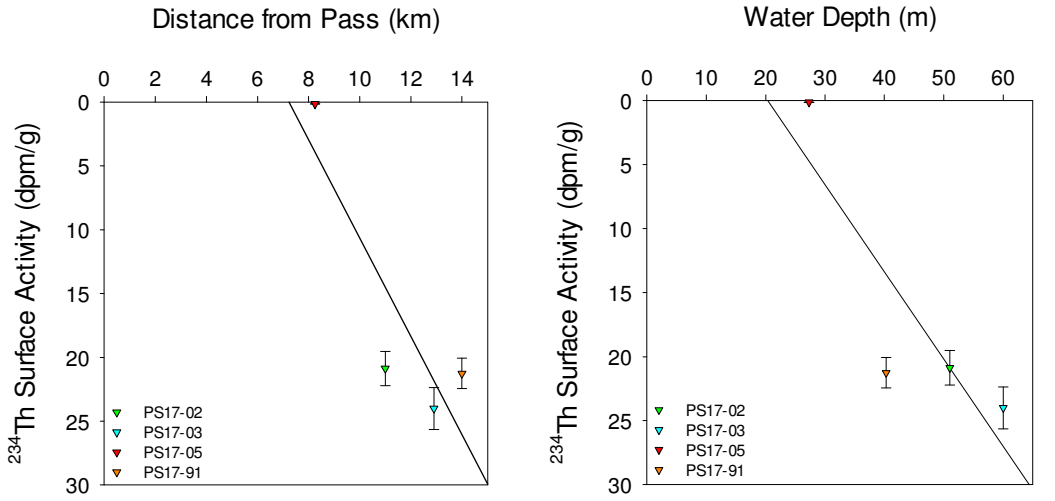

A4: Excess ^{234}Th surface activity (dpm/g) versus distance from pass (km), R^2= 0.77 (left); and water depth (m), R^2= 0.76 (right). Samples analyzed for ^{234}Th are denoted by upside down triangles.

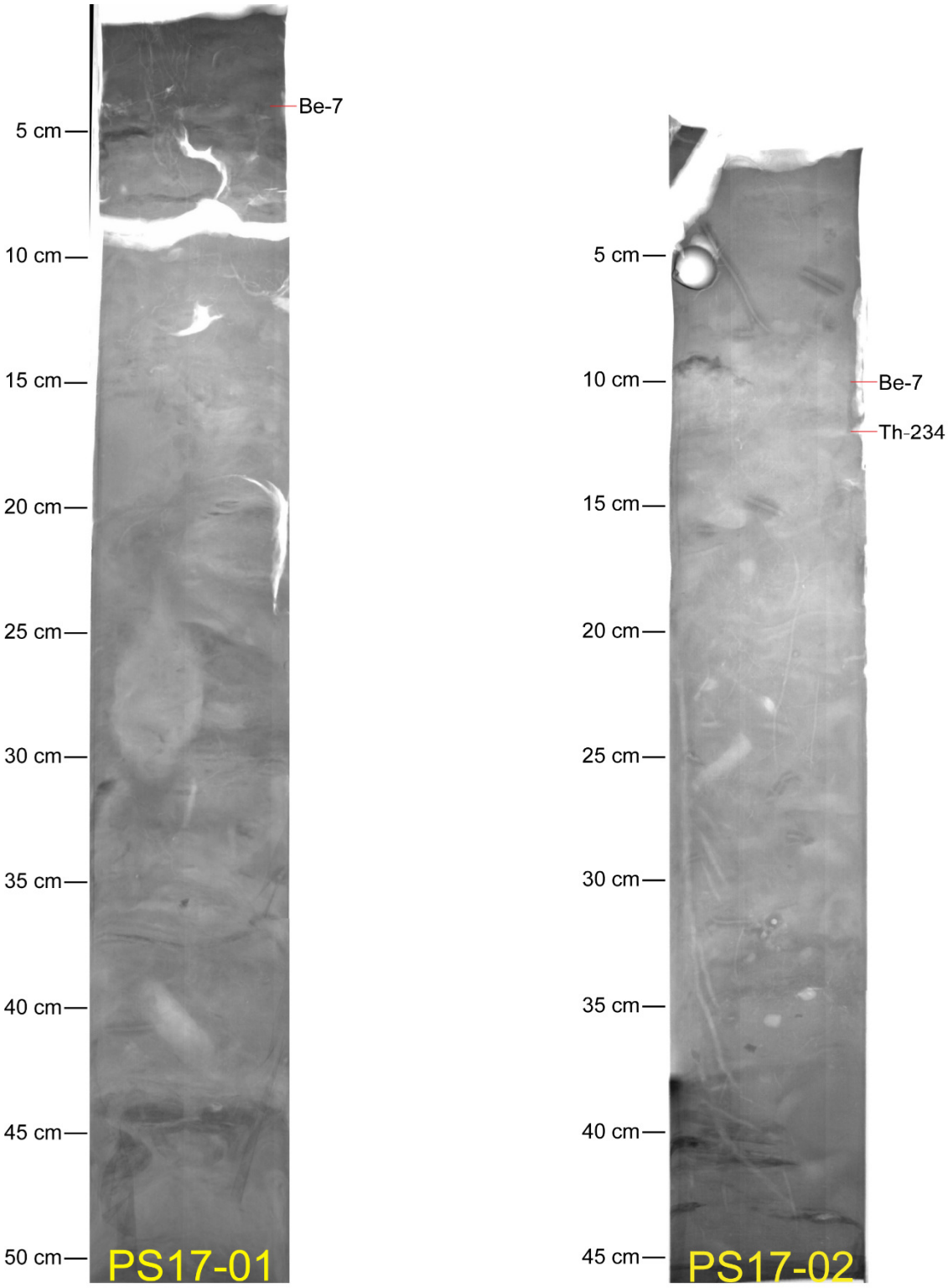

A5: X-radiograph images of core locations off SW Pass. ^{7}Be and $^{234}Th_{xs}$ penetration depths labeled. Depth (cm) down core labeled at 5 cm intervals. Water depth for PS17-01 (undisturbed) is ~ 31 m and PS17-02 (gully) is ~ 51 m.

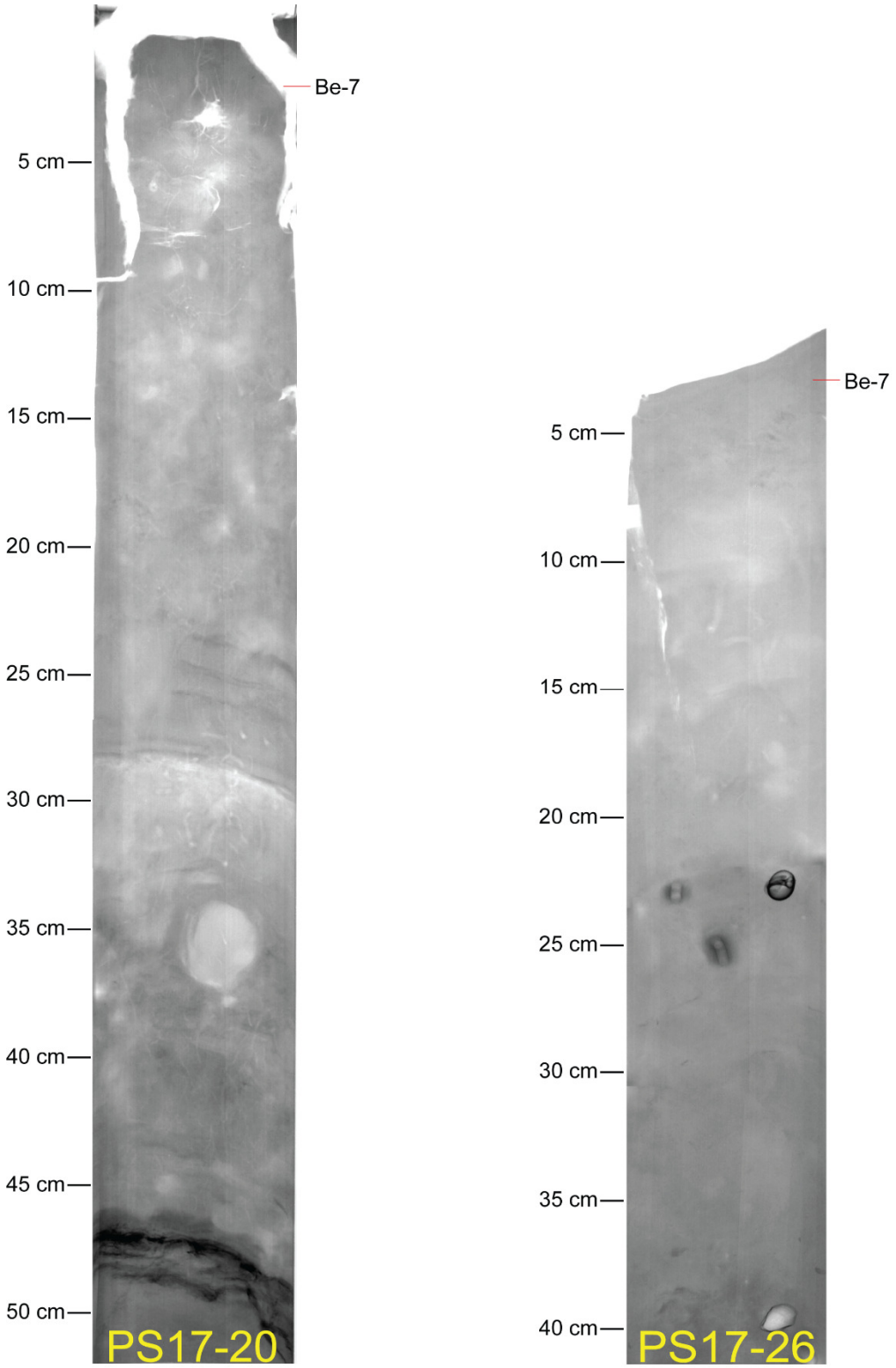

A6: X-radiograph images of core locations off S Pass. ^{7}Be penetration depths labeled. Depth (cm) down core labeled at 5 cm intervals. Water depth for PS17-20 (undisturbed) is ~ 187 m and PS17-26 (undisturbed) is ~ 206 m.

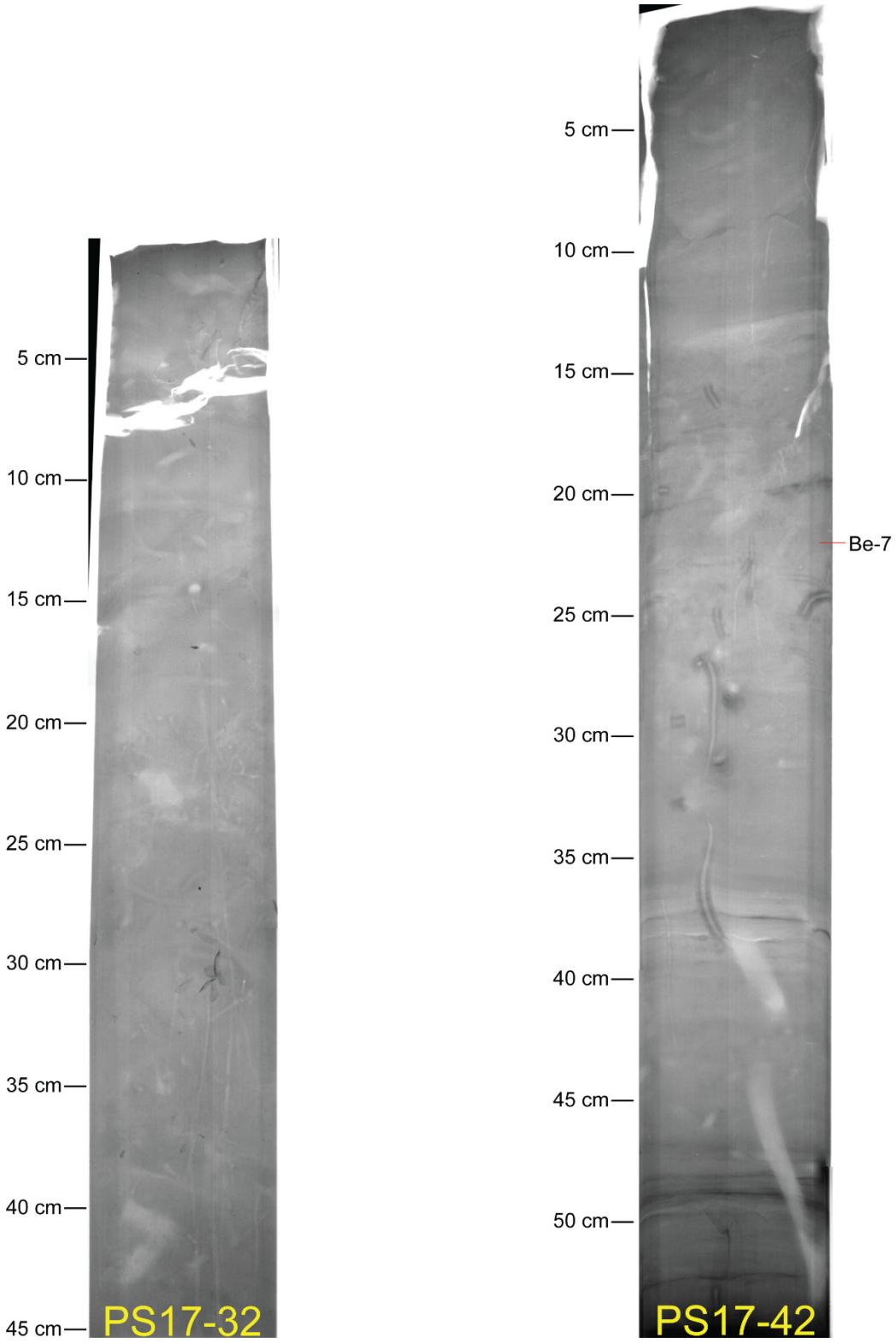

A7: X-radiograph images of core locations off S Pass. ^{7}Be penetration depths labeled. Depth (cm) down core labeled at 5 cm intervals. Water depth for PS17-32 (prodelta) is ~ 258 m and PS17-42 (gully) is ~ 39 m. ^{7}Be was not detected in core PS17-32.

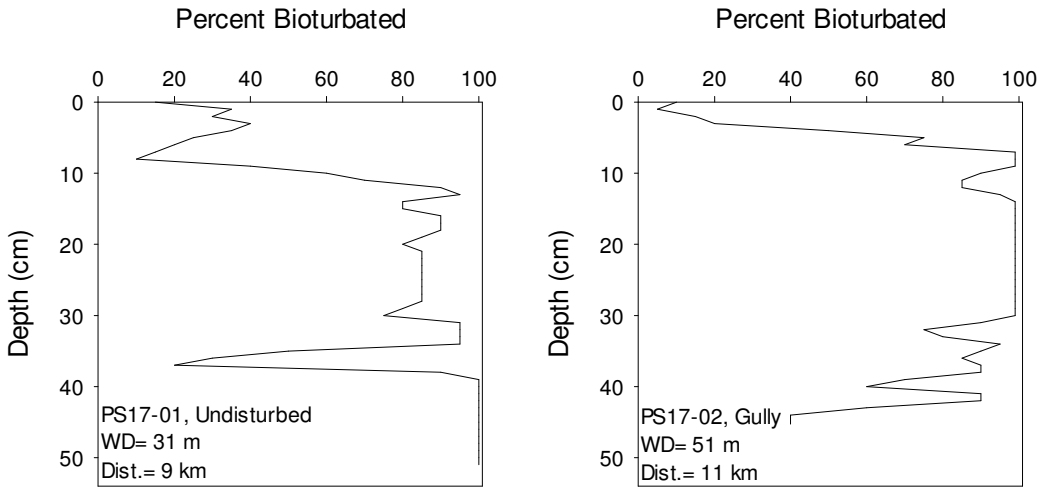

A8: Plots of percentage of sedimentary fabric bioturbated of cores off SW Pass (PS17-01, PS17-02). Observations made at 1 cm intervals.

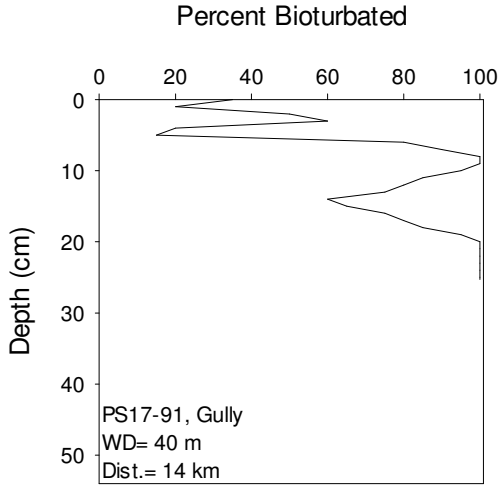

A9: Plots of percentage of sedimentary fabric bioturbated of cores off PAL (PS17-91). Observations made at 1 cm intervals.

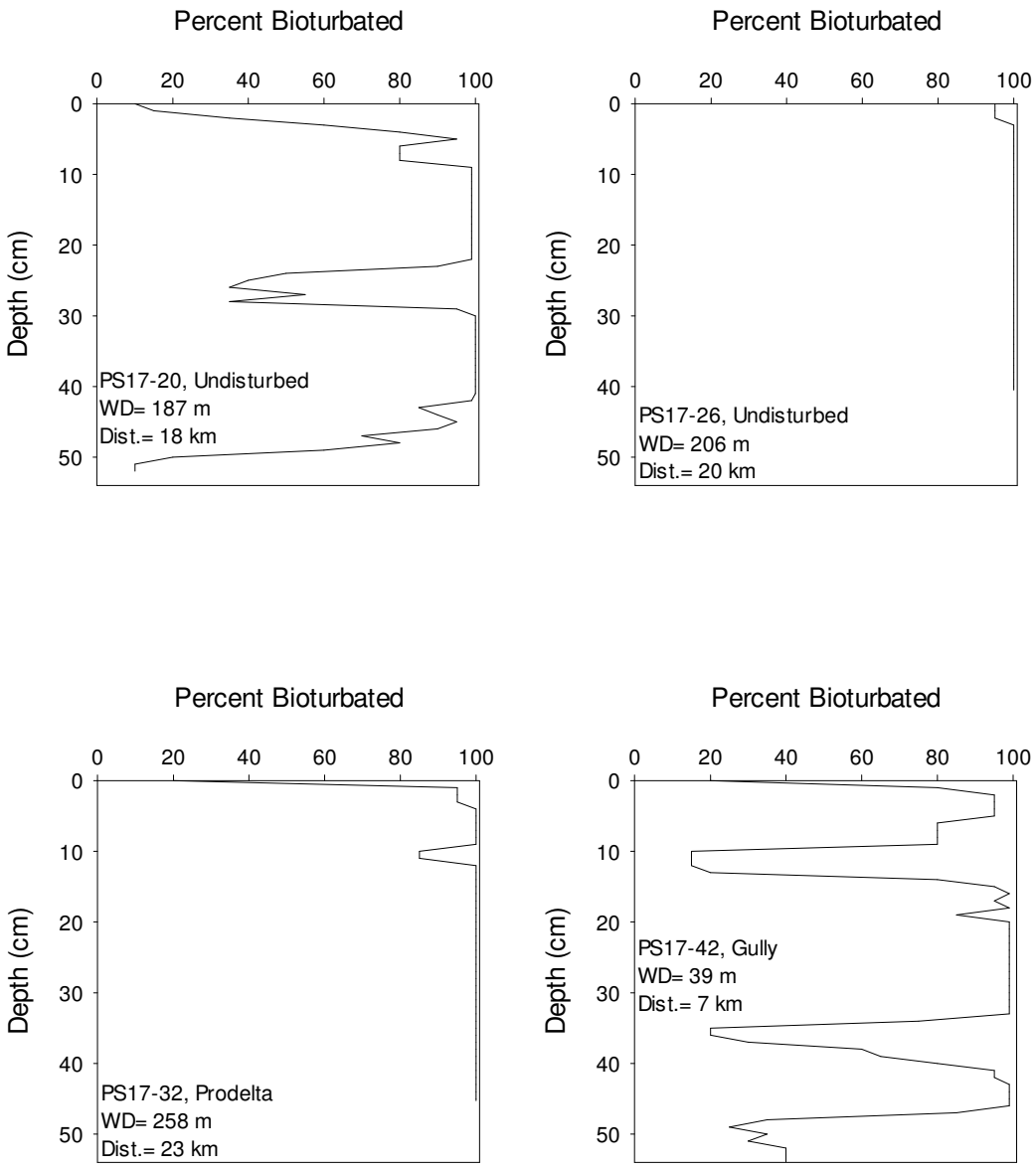

A10: Plots of percentage of sedimentary fabric bioturbated of cores off S Pass (PS17-20, PS17-26, PS17-32, PS17-42). Observations made at 1 cm intervals.

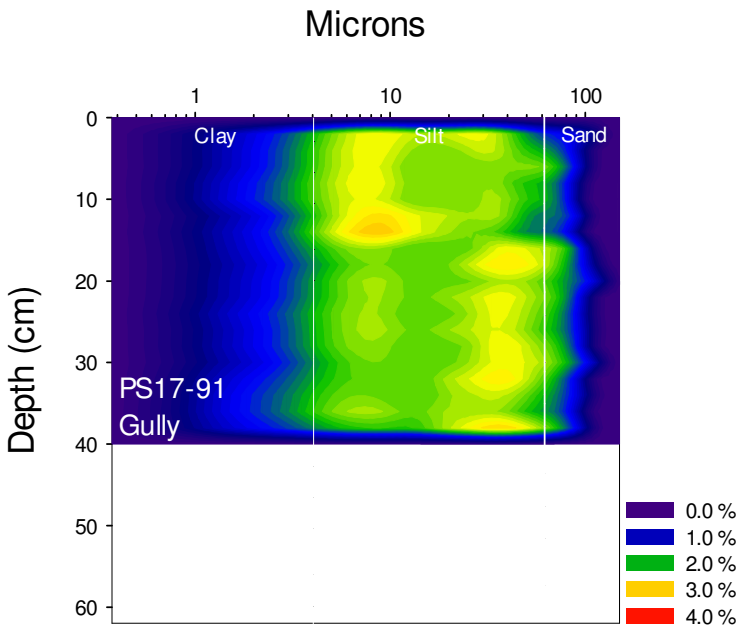

A11: Pass a Loutre grain-size plot by percent volume occurrence (0-4%). Clay, silt, and sand size ranges are denoted by vertical white lines.

Vita

Andrew Courtois was born and raised in Louisiana and always had a passion for the outdoors. Growing up hunting and fishing in coastal Louisiana he was taught to care for the land. Over the past few years, his work has revolved around coastal research. After graduation, he plans to use his knowledge and experience in pursuing a career in coastal research.